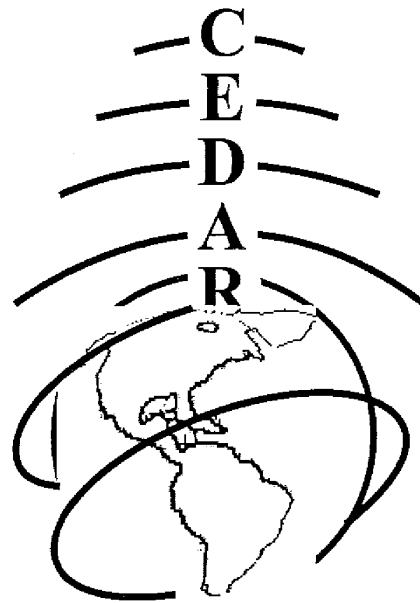




EDAR-GEM Joint Workshop

Santa Fe, New Mexico
June 19 - June 24, 2016



CEDAR MLT Poster Session Booklet
Wednesday, June 22, 2016



Table of Contents

Coupling of the Upper Atmos with Lower Altitudes

COUP-01	Cornelius Csar Jude Salinas, Impacts of Global Mean CO ₂ -based Eddy Diffusion Coefficients in the Mesosphere and Lower Thermosphere Region on the Ionosphere/Thermosphere Region	1
COUP-02	Loren Chang, Observations and modelling of quasi-biennial variations in ionospheric tidal/SPW amplitudes	1
COUP-03	Christopher Krier, Nonmigrating tidal impacts on the [O]/[N ₂] ratio in GUVI	2
COUP-04	Robert Anthony Haaser, Exploring the atmospheric and ionospheric response to bolides in the Earth's atmosphere	2
COUP-05	Vu Nguyen, Interannual Variability of Secondary Waves Arising from QTDW-DW1 Interaction	3
COUP-06	Joe McInerney, Recent Enhancements of the Whole Atmosphere Community Climate Model - eXtended (WACCM-X)	3
COUP-07	Rafael Mesquita, The midnight temperature maximum in the mid-latitude NATION network.....	3
COUP-08	McArthur Jones Jr., Contributions of lower atmospheric drivers to the semiannual and annual oscillations in thermospheric global mass density	4
COUP-09	Matthew Grawe, Observation of Tsunami-Generated Ionospheric Signatures in Hawaii from the 16 September 2015 Illapel Earthquake	4
COUP-10	Cissi Lin, A study of the nonlinear response of the upper atmosphere to episodic and stochastic acoustic-gravity wave forcing	5
COUP-11	Federico Gasperini, Synthetic thermosphere winds based on CHAMP neutral and plasma density measurements	5
COUP-12	Federico Gasperini, Solar EUV effects on the vertical propagation of waves from the lower to the middle thermosphere as viewed from TIMED and GOCE	6
COUP-13	Jessica Hawkins, WN4 Variability in the Topside Ionosphere	6
COUP-14	Greg Lucas, Solar impacts on atmospheric electric fields	6

Instruments or Techniques for Middle Atmosphere Observations

ITMA-01	Marcos Inonan, Inferring ratio of negative ion to electron concentration by using Arecibo Incoherent Scatter Radar	7
ITMA-02	Irfan Azeem, Super Soaker: A Sounding Rocket Mission to Study Transport, Chemistry, and Energetics of Water in the Mesosphere and Lower Thermosphere and Implications for Polar Mesospheric Cloud Occurrence	7
ITMA-03	Jackson C. McCormick, Spatial and Temporal Ionospheric Monitoring Using Broadband Sferics	8

ITMA-04	Jih-Chin Lai, INSPIRESat-1: Introduction and Feasibility Study for a CubeSat Mission for Middle and Upper Atmosphere Wind and Temperature Observations .8
ITMA-05	Jintai Li, Studies of Turbulence in the Arctic Mesosphere with PFISR9
ITMA-06	Preston Hooser, Thermospheric Temperature Analysis Methods for the OPAL Mission9
ITMA-07	Jens Lautenbach, Proposing an upgrade of the Arecibo lidar systems to enhance science capabilities10

Long Term Variations of the Mesosphere and Lower Thermosphere

LTVM-01	Bing Cao, Intermittency of Gravity Waves Momentum Flux in Airglow Imager Observations and Whole Atmosphere Community Climate Model (WACCM) ... 10
LTVM-02	Gawon Kim, An analysis of long-term trends in mesospheric temperatures from OH airglow spectra of Kiruna FTS and Sloan Digital Sky Survey 10

Meteor Science other than wind observations

METR-01	Andrew Nuttall, Radio-Frequency Emissions from Hypervelocity Meteoroid Impacts 11
METR-02	Liane Kathryn Tarnecki, Spectra of Full 3-D PIC Simulations of Turbulent Meteor Trails11
METR-03	Glenn Sugar, Particle In Cell Simulation of Meteor Head Echo 12
METR-04	Freddy Ronald Galindo, Effect of Plasma Turbulence on the evolution of Specular Meteor Echoes 12
METR-05	Diana Juarez Madera, Size Distribution Of Fragmented Grains From The Intensity And Duration Of Meteor Flares 12
METR-06	Lorenzo Limonta, Detection and Characterization of Meteoroid From Optical and Radar Observations 13

MLT Gravity Waves

MLTG-01	Ahmad Talaei, Investigating Seasonal Mesospheric Gravity Wave Propagation and Variability 13
MLTG-02	Pattilyn Frances McLaughlin, DEEPWAVE: Ground-based analysis of Mesospheric Gravity Wave Signatures 13
MLTG-03	Jaime Aguilar, Synthetic Airglow All-Sky Imager Data for the Interpretation of Gravity Waves Imaged Over Wide Fields of View 14
MLTG-04	Thomas Lobay, Modeling of mountain-generated gravity waves 14
MLTG-05	Dhvanit Mehta, Mesospheric Gravity Waves and their Sources at the South Pole. 15
MLTG-06	Robert Bruntz, Modeling atmospheric gravity waves using the Transfer Function Model (TFM) and the associated ionospheric responses 15

MLTG-07	Cao Chen, Two-dimensional Morlet wavelet transform and its application to extracting two-dimensional wave packets from lidar observations in Antarctica...	15
MLTG-08	Tyler Mixa, Gravity Wave Instability Evolution in Variable Stratification and Shear	16
MLTG-09	Andrew J. Kavanagh, First Observations from the February 2016 World Day on Gravity Waves	16
MLTG-10	Yolian Amaro-Rivera, Comparison of gravity wave induced airglow variations using MSIS-90 and NRLMSISE-00 atmospheric density models	17

MLT Lidar Studies

MLTL-01	Jonathan Price, Obtaining Continuous Observations from the Upper Stratosphere to the Lower Thermosphere Using the ALO-USU Rayleigh-Scatter Lidar	17
MLTL-02	Leda Sox, Simultaneous, collocated Rayleigh and sodium lidar temperature comparison	17
MLTL-03	Vincent B. Wickwar, Seasonal Temperatures from the Upper Mesosphere to the Lower Thermosphere Obtained with the Large, ALO-USU Rayleigh Lidar	18
MLTL-04	Shayli Elliott, Reestablishing Observations throughout the Mesosphere with the ALO-USU Rayleigh-Scatter Lidar	18
MLTL-05	David K. Moser, Searching for Troposphere-Mesosphere Connections Using the ALO-USU Rayleigh-Scatter Lidar	19
MLTL-06	Jian Zhao, Characterization of gravity waves in the stratosphere and lower mesosphere at McMurdo, Antarctica	19
MLTL-07	Luis Navarro, First results from new observational capabilities of the Na Lidar at Utah State University	19
MLTL-08	Luis Navarro, Latitudinal variations on winds and temperature between ALO and USU Na Lidars	19
MLTL-09	Shuai Qiao, Variations in mesospheric densities from Rayleigh lidar observations at Golmud	20
MLTL-10	Xian Lu, Statistical characterization of high-to-medium frequency gravity waves in vertical winds and temperatures measured by lidar in the MLT	20
MLTL-11	Yafang Guo, Gravity Wave and Turbulence Transport of Heat and Na in the Mesopause Region over the Andes	21
MLTL-12	Chao Ban, Lidar observation of thermosphere sodium layers at Andes Lidar Observatory (30.25° S, 70.74° W)	21
MLTL-13	Anthony Lima, Investigation of vertical wavenumber and frequency and spectra of gravity wave motions using vertical wind measurements at Boulder.....	21

Mesosphere or Lower Thermosphere General Studies

MLTS-01	Jing Li, Characteristics of ripple structures revealed from long-term OH airglow images	22
----------------	-----------------------------------------------------------------------------------------------	----

MLTS-02	Jaroslav Jansky, Effects of conductivity perturbations in time dependent global electric circuit model	22
MLTS-03	Jaroslav Jansky, Analysis of the diurnal variation of the global electric circuit using different numerical models	23
MLTS-04	Jaroslav Jansky, Earthquake lights: Mechanism of energetic coupling of Earth's crust to the lower atmosphere	23
MLTS-05	Yi Chung Chiu, Development and Validation of an Airglow Photometer for Upper Atmospheric Chemistry	23
MLTS-06	Jonathan S. Friedman, Metal layers in the thermosphere at Arecibo	24
MLTS-07	Christian Tate, Analysis of Mesospheric Inversion Layers from eCMAM30 (1979 - 2010)	24

MLT Other Tidal, Planetary Waves, or Sudden Stratospheric Warmings

MLTT-01	Ashan Vitharana, A comparison of statistical properties of diurnal tides between eCMAM30 and SABER	24
MLTT-02	Hongping Gu, Physical Mechanisms of Seasonal Variation of DW1 from the Stratosphere to Thermosphere in eCMAM30	25
MLTT-03	Ryan Agner, Parameterized Gravity Wave Effects on Major Tidal Modes in eCMAM and WACCM	25
MLTT-04	Jeong Han Kim, Vertical structures of temperature change in the mesosphere and lower thermosphere regions during stratospheric sudden warnings	25
MLTT-05	Nirmal Nischal, Nonmigrating tidal impact on the CO ₂ 15 μm infrared cooling of the lower thermosphere over one solar cycle	26

Sprites

SPRT-01	Jacob Allen Engle, Numerical and analytical studies of critical radius in spherical and cylindrical geometries for corona discharge	26
SPRT-02	Mohammad Ahmad Salem, The Electrical Impact of Sprite Halos on the Nighttime Lower Ionosphere	27

Stratosphere Studies and Below

STRA-01	Chengyun Yang, The northern stratospheric temperature response to MJO in cases SSW occurs or not	28
STRA-02	Levi Boggs, Thunderstorm Charge Structures Producing Negative Gigantic Jets..	28

CEDAR Workshop – MLT Poster Session Abstracts

Day 2 – Wednesday, June 22, 2016

Coupling of the Upper Atmosphere with Lower Altitudes

COUP-01 - Impacts of Global Mean CO₂-based Eddy Diffusion Coefficients in the Mesosphere and Lower Thermosphere Region on the Ionosphere/Thermosphere Region - by Cornelius Cesar Jude Salinas

Status of First Author: Student IN poster competition, PhD

Authors: Loren C. Chang, Mao-chang Liang, Jia Yue, James Russel III

Abstract: In this work, SABER/TIMED observations of monthly global-mean CO₂ profiles and a 1D model are used to estimate eddy diffusion coefficients (K_{zz}). At 98 km, global mean CO₂ shows both an annual oscillation (AO) and a semiannual oscillation (SAO) with maximum during solstice seasons along with a primary and secondary minimum in boreal spring and fall, respectively. Our calculated AO and SAO in global-mean CO₂ is modeled by an AO and SAO in K_{zz}. Our CO₂-based K_{zz} at 98 km are then utilized for the lower boundary condition in the Thermosphere-Ionosphere Electrodynamics General Circulation Model (TIE-GCM). Our output runs show that the CO₂-based K_{zz} does not induce the observed AO and SAO in Thermospheric composition, density and NmF₂ and HmF₂. From these modeling experiments along with a comparison of our CO₂-based K_{zz} with satellite-drag/GUVI (Global Ultra-violet Imager) observations-based K_{zz} and with recently improved K_{zz} in the Specified Dynamics- Whole Atmosphere Community Climate Model (SD-WACCM), our work concludes that our CO₂-based K_{zz} may represent eddy diffusion solely due to gravity wave mixing. Furthermore, our work suggests that the discrepancy between our CO₂-based K_{zz} and satellite-drag/GUVI observations-based K_{zz} represents diffusion from other unspecified sources.

COUP-02 - Observations and modelling of quasi-biennial variations in ionospheric tidal/SPW amplitudes - by Loren Chang

Status of First Author: Non-student, PhD

Authors: Yan--Yi Sun, Jack Chieh Wang, Jia Yue, Qian Wu, Shih--Han Chien

Abstract: In this study, we examine the coherent spatial and temporal modes dominating the variation of selected ionospheric tidal and stationary planetary wave signatures from 2007-2013 FORMOSAT-3/COSMIC total electron content observations using Multi-dimensional Ensemble Empirical Mode Decomposition (MEEMD) from the Hilbert--Huang Transform. We examine the DW1, SW2, DE3, and SPW4 components, which are driven by a variety of in--situ and vertical coupling sources. The intrinsic mode functions (IMFs) resolved by MEEMD analysis allows for the isolation of the dominant modes of variability for prominent ionospheric tidal / SPW signatures in a manner not previously used, allowing the effects of specific drivers to be examined individually.

The time scales of the individual IMFs isolated for all tidal/SPW signatures correspond to a semiannual variation at EIA latitudes maximizing at the equinoxes, as well as annual oscillations at the EIA crests and troughs. All tidal / SPW signatures show one IMF isolating an ionospheric quasi-biennial oscillation (QBO) in the equatorial latitudes maximizing around January of odd numbered years. This TEC QBO variation is in phase with a similar QBO variation isolated in both the GUVI zonal mean column O/N₂ density ratio as well as the F10.7 solar radio flux index around solar maximum, while showing temporal

variation more similar to that of GUVI O/N₂ during the time around the 2008/2009 extended solar minimum. These results point to both quasi-biennial variations in solar irradiance as well as thermosphere / ionosphere composition as a generation mechanism for the ionospheric QBO. Numerical experiments using TIE-GCM show that the majority of the ionospheric QBO can be attributed to solar irradiance, with mixing from modulated MLT tides playing a secondary role.

COUP-03 - Nonmigrating tidal impacts on the [O]/[N₂] ratio in GUVI - by Christopher Krier

Status of First Author: Student IN poster competition, Undergraduate

Authors: Christopher Krier, Jens Oberheide, Nirmal Nischal (all Clemson University), Yongliang Zhang (Johns Hopkins University)

Abstract: Our main objective is to study the impact of nonmigrating tides forced by large-scale tropical convection on the composition of the thermosphere using [O]/[N₂] column density ratios observed by the GUVI instrument on board the TIMED satellite. The [O]/[N₂] column density ratio is referenced to a N₂ column density of 1017 cm⁻² (vicinity of 135 km). As such, [O]/[N₂] should be a sensitive measure for upward (depressed ratio) and downward (enhanced ratio) motions caused by upward propagating tides. Indeed, the GUVI data show large “wave-4” like [O]/[N₂] perturbations on the order of 15% (peak-to-peak) but their propagation direction in the local time frame is inconsistent with the expectation from tidal theory: the GUVI wave-4 mainly propagates westward while the theoretical prediction is a tidal eastward propagation caused by the DE3 and SE2 nonmigrating tides. To understand this surprising behavior, we perform a number of model simulations using NRLMSISE-00 background and tides from the TIMED-based empirical CTMT tidal model. Our results indicate that a large part of the [O]/[N₂] “wave-4” signal originates in the ionosphere, that is, from 135.6 nm emissions from “wave-4” like plasma density variations in the F-region. We discuss the relative importance of this ionospheric contamination as a function of local time to isolate the “true” impact of nonmigrating tides on the [O]/[N₂] variability in the thermosphere.

COUP-04 - Exploring the atmospheric and ionospheric response to bolides in the Earth's atmosphere - by Robert Anthony Haaser

Status of First Author: Non-student, PhD

Authors: Robert A. Haaser, Erin H. Lay, William Junor

Abstract: Impulsive phenomena such as earthquakes, volcanic eruptions, ground explosions, and objects entering the Earth's atmosphere produce acoustic (compression) and gravity (buoyant) waves which propagate through the atmosphere and produce seismic signatures, infra-sound waves at ground level, and electron density fluctuations at ionospheric altitudes. When energetic enough, atmospheric waves can be measured via Total Electron Content (TEC), derived from ground-based Global Positioning System (GPS) phase data. GPS-TEC is the most widely, publicly available resource for remote ionosphere observation data. Since the ionospheric densities are highest at altitudes near 350 km, each connecting line between any ground station (local to an event of interest) and any available GPS satellite effectively scans the ionosphere at that altitude. This method can provide a significant amount of information on the location and nature of wave sources driving fluctuations in the ionosphere. In this work, atmospheric waves resulting from bolides are explored via GPS-TEC, and compared to other sample impulsive cases. A bolide is an object, natural or man-made, that enters the atmosphere with enough energy to become incandescent, brighter than the full moon, audible at the ground, exploding due to rapid thermal expansion before reaching the ground (usually above 15 km), and leaving tangible meteorites/pieces on the ground. Though previous attention has been paid to a small number of high-profile bolide cases, like the Chelyabinsk Bolide of 2003, this work includes a more extensive exploration of the general nature of ionospheric signatures of bolides. Here, we present methodologies and results thus far.

COUP-05 - Interannual Variability of Secondary Waves Arising from QTDW-DW1 Interaction - by Vu Nguyen

Status of First Author: Student IN poster competition, Masters

Authors: Vu Nguyen, Ruth Lieberman, Scott Palo

Abstract: Theory and past observations have provided evidence that atmospheric tides and other global scale waves may nonlinearly interact to produce additional secondary waves throughout the space-atmosphere interaction region. However, very few studies have investigated the generation region of nonlinearly secondary waves, and as a result the manifestations and impacts of these waves are still poorly understood. This study focuses on the nonlinear interaction between the quasi two-day wave (QTDW) and the migrating diurnal tide (DW1), two of the largest global scale waves in the atmosphere. The fundamental goal of this effort is to fully understand the factors that influence secondary wave response in the space-atmosphere interaction region (SAIR). First, momentum and thermal forcing for each secondary wave are derived from the NOGAPS-ALPHA reanalysis model. These quantities are used to force a linear tidal model in order to calculate secondary wave responses. The modeling results to be presented are used to investigate how the effects of the nonlinear forcing, background winds and interannual variability influence the secondary wave response in the SAIR.

COUP-06 - Recent Enhancements of the Whole Atmosphere Community Climate Model - eXtended (WACCM-X) - by Joe McInerney

Status of First Author: Non-student, Masters

Authors: Joe McInerney, Ben Foster, Hanli Liu, Stan Solomon, Dan Marsh, Liying Qian, Wenbin Wang, Art Richmond, Gang Lu, Astrid Maute, Mike Wiltberger

Abstract: The next release of the Community Earth System Model (CESM) is scheduled for December of this year. This release will include a functional version of the Whole Atmosphere Community Climate Model - eXtended (WACCM-X) with a more thorough ionosphere and thermosphere. This model is being developed at the National Center for Atmospheric Research (NCAR) High Altitude Observatory (HAO) in Boulder, Colorado and is based on the Whole Atmosphere Community Climate Model (WACCM) and the Community Atmosphere Model (CAM), which make up the atmospheric component of CESM. While CAM extends from the ground to ~30 km and WACCM to ~140 km, WACCM-X has a model top of ~600 km. Here we give a flavor of what to expect in this upcoming WACCM-X release and developments to be included in future releases.

COUP-07 - The midnight temperature maximum in the mid-latitude NATION network - by Rafael Mesquita

Status of First Author: Student IN poster competition, PhD

Authors: Rafael Mesquita, John Meriwether, Jonathan Makela, Daniel Fisher, Samuel Sanders, Brian Hardin.

Abstract: In this work, the results of Fabry-Perot interferometer (FPI) measurements of thermospheric temperatures and winds show the detection and successful determination of the latitudinal distribution of the midnight temperature maximum (MTM) in the continental mid-eastern United States. These results were obtained from the simultaneous operation of the five FPI observatories that constitute the North American Thermosphere Ionosphere Observing Network (NATION). These sites are the Pisgah Astronomic Research Institute (PAR) (35.2 N, 82.8 W), Virginia Tech (VTI) (37.2 N, 80.4 W), Eastern Kentucky University (EKU) (37.8 N 84.3 W), Urbana-Champaign (UAO) (40.1 N 88.2 W) and Ann Arbor (ANN) (42.3 N 83.8 W). The analysis of these observations found the MTM structure to exhibit a strong variability from night to night, with this feature not present in many of the nights in the NATION database.

A statistical study of the behavior of the MTM events examined this variability in regard to the seasonal and latitudinal dependence. The results obtained indicate that the MTM peak was detected in 106 out of the 472 nights (22%) selected for study out of the total of 846 nights analyzed. The other nights were not used in this study because the data sets were incomplete with data from fewer than 5 sites. The MTM feature is seen to appear slightly more often during the summer (27%), followed by fall (22%), winter (20%) and spring (18%). Also seen is a northeast-ward propagation of the MTM structure with variable amplitude along the path from the southwest toward the northeast over a range of 1400 km (from 33 N to 44 N). One explanation for this finding is the existence of a latitudinal distribution of thermosphere tidal dissipation. Another possibility is a latitudinal variation of the blending together of the higher order tidal modes that contribute to the production of the MTM peak. This explanation would account for why the amplitude of this MTM structure varies from night to night or is non-existent. This work also features a method of 2D interpolation and the extraction of the background temperature variation for the baseline of the MTM structure.

COUP-08 - Contributions of lower atmospheric drivers to the semiannual and annual oscillations in thermospheric global mass density - by McArthur Jones Jr.

Status of First Author: Non-student, PhD

Authors: John T. Emmert, Douglas P. Drob

Abstract: Annual and semiannual oscillations (AO and SAO) are collectively the second largest component, after solar variability, of thermospheric global mass density variations. Several mechanisms have been proposed to explain the oscillations, but they have yet to be reproduced by first-principles modeling simulations. The leading hypothesis is that intra-annual variations (IAV) in lower thermospheric turbulent mixing (associated with breaking gravity waves) modulate upper thermospheric composition. Recent studies have focused on estimating the IAV in eddy diffusion required to explain the thermospheric IAV in mass density. Less attention has been paid to the effect of lower and middle atmospheric drivers on the lower boundary of the thermosphere. In particular, the connections among gravity waves, atmospheric tides, and IAVs near the turbopause and in the upper thermosphere have not yet been considered in first principles modeling simulations. In this study, we utilize the National Center for Atmospheric Research Thermospheric General Circulation Models (TGCs), to elucidate how the different lower atmospheric drivers influence the IAV of globally-averaged thermospheric mass density. Numerical experiments are performed for 2009 assuming constant solar and geomagnetic forcing, in which we modify the eddy diffusion and the lower boundary temperature, winds, and composition, including tides thereof, in order to quantify the AO and SAO in thermospheric mass density attributable to different lower atmospheric drivers.

COUP-09 - Observation of Tsunami-Generated Ionospheric Signatures in Hawaii from the 16 September 2015 Illapel Earthquake - by Matthew Grawe

Status of First Author: Student IN poster competition, Masters

Authors: Matthew Grawe, Jonathan Makela

Abstract: Tsunamis generate internal gravity waves (IGW) as they propagate that produce detectable signatures in the ionosphere. These signatures have consistently been observed in the presence of a tsunami for over a decade in the total electron content and for over five years in the 630.0 nm airglow. Here, we show perturbations appearing in the filtered TEC and 630.0 nm airglow above Hawaii during the passing of the tsunami induced by the 16 September, 2015 earthquake in Illapel, Chile. We report wave measurements from both observation methodologies using a combination of prior methods and a newer method that uses a Gabor filter bank. A previously developed geometric model that takes into account the posture of tsunami-induced IGWs in the geomagnetic field and the observation geometry is shown to predict fairly well the expected location of the observation in the sky. Results are also compared to signatures from the March 2011 Tohoku and October 2012 Haida Gwaii events.

COUP-10 - A study of the nonlinear response of the upper atmosphere to episodic and stochastic acoustic-gravity wave forcing - by Cissi Lin

Status of First Author: Non-student, PhD

Authors: Cissi Y. Lin, Yue Deng, Cheng Sheng, Douglas P. Drob

Abstract: Perturbations caused by geophysical and anthropogenic events on the ground have been observed to propagate upward and impact the upper atmosphere. It is known that gravity waves with wavelengths less than 750 km are responsible for these total electron content (TEC) perturbation and play a significant role in the mass, momentum, and energy budgets of the mesosphere and lower thermosphere (MLT). These waves are however difficult to continuously measure, globally resolve, and deterministically specify in first-principle ionosphere-thermosphere (IT) models. In this study, we investigate nonlinear IT response to induced acoustic-gravity waves (AGWs) resulting from time-varying lower atmospheric wave forcing, including a traveling wave packet (TWP) and stochastic gravity wave (SGW) fields using the Global Ionosphere Thermosphere Model (GITM) with high-resolution grids of 0.08° in longitude and latitude. When TWP and SGW forcing occurs concurrently, the induced gravity waves (GWs) cause variation of $\pm 8.8\%$ in neutral, $\pm 6.2\%$ in electron density, and $\pm 1.5\%$ in TEC. The magnitudes decrease by 2.2% (for example, from $\pm 8.8\%$ to $\pm 6.6\%$) under a TWP-only scenario and importantly nonlinear interactions between TWP and SGW contribute to $\pm 1.4\%$ of the perturbations. On the other hand, the induced acoustic waves (AWs) cause variation of $\pm 13.9\%$ in neutral, $\pm 2.1\%$ in electron density, and $\pm 0.4\%$ in TEC. Furthermore, GWs sustain tens of minutes after the TWP has passed through the lower atmosphere and clear TIDs and TADs are developed. We demonstrate that clear wave structures from an episodic event can be isolated even under a ubiquitously and overwhelmingly perturbed atmosphere.

COUP-11 - Synthetic thermosphere winds based on CHAMP neutral and plasma density measurements - by Federico Gasperini

Status of First Author: Student IN poster competition, PhD

Authors: Federico Gasperini, Jeffrey Forbes, Eelco Doornbos, Sean Bruinsma

Abstract: Meridional winds in the thermosphere are key to understanding latitudinal coupling and thermosphere-ionosphere coupling, and yet global measurements of this wind component are scarce. In this work, neutral and electron densities measured by the Challenging Minisatellite Payload (CHAMP) satellite at solar low and geomagnetically quiet conditions are converted to pressure gradient and ion drag forces, which are then used to solve the horizontal momentum equation to estimate low- to mid-latitude zonal and meridional 'synthetic' winds. We validate the method by showing that neutral and electron densities output from National Center for Atmospheric Research (NCAR) Thermosphere Ionosphere Mesosphere Electrodynamics-General Circulation Model (TIME-GCM) can be used to derive solutions to the momentum equations that replicate reasonably well (over 85% of the variance) the winds self-consistently calculated within the TIME-GCM. CHAMP cross-track winds are found to share over 65% of the variance with the synthetic zonal winds, providing further reassurance that this wind product should provide credible results. Comparisons with the Horizontal Wind Model 14 (HWM14) show that the empirical model largely underestimates wind speeds and does not reproduce much of the observed variability. Additionally, in this work we: reveal the longitude, latitude, local time, and seasonal variability in the winds; show evidence of ionosphere-thermosphere (IT) coupling, with enhanced post-sunset eastward winds due to depleted ion drag; demonstrate superrotation speeds of ~ 27 m/s at the equator; discuss vertical wave coupling due the diurnal eastward propagating tide with zonal wavenumber 3 (DE3) and the semidiurnal eastward propagating tide with zonal wavenumber 2 (SE2).

COUP-12 - Solar EUV effects on the vertical propagation of waves from the lower to the middle thermosphere as viewed from TIMED and GOCE - by Federico Gasperini

Status of First Author: Non-student, PhD

Authors: Federico Gasperini, Jeffrey Forbes, Eelco Doornbos , Sean Bruinsma

Abstract: The vertical coupling of waves from the lower to the middle thermosphere is a key process in determining the dynamics and electrodynamics of the upper atmosphere system. In this work, the effect of solar radiation on the vertical propagation of the eastward propagating diurnal tide with zonal wavenumber 3 (DE3) is investigated using Thermosphere, Ionosphere, Mesosphere, Energetics and Dynamics-Sounding of the Atmosphere using Broadband Emission Radiometry (TIMED-SABER) temperatures near 110 km and Gravity field and steady-state Ocean Circulation Explorer (GOCE) neutral densities and zonal winds near 260 km. The analysis is performed at low to mid-latitudes during 2010-2012, when reliable and continuous measurements are available. We decompose DE3 into its equatorially symmetric and anti-symmetric components, and use Hough Mode Extensions (HMEs) to convert DE3 temperatures at 110 km to DE3 densities at 110 km. By least squares fitting DE3 density at 260 km to DE3 density at 110 km and S10.7, we separate the variation in DE3 at 260 km into the part due to vertical extension from 110 km and the part due to variable dissipation. To characterize the effect of solar EUV on the vertical propagation of DE3, we then perform correlation analyses between day-to-day variations in DE3 symmetric and variations in the S10.7 EUV index (26-34 nm).

COUP-13 - WN4 Variability in the Topside Ionosphere - by Jessica Hawkins

Status of First Author: Student IN poster competition, PhD

Authors: Jessica M. Hawkins, Phillip C. Anderson

Abstract: Atmospheric tides are global-scale periodic oscillations of the atmosphere, with scale sizes of thousands to tens of thousands of kilometers. Non-migrating tides, which do not follow the apparent motion of the Sun, can significantly alter the global ionospheric structure. In particular the wave-number 4 (WN4) pattern, which has four peaks equally spaced in longitude when viewed in a constant local time frame, is thought to be a signature of the DE3 non-migrating tide propagating upward from the lower atmosphere, and is therefore an important clue to whole-atmosphere coupling. While DE3 and WN4 signatures have been much studied in recent years in the mesosphere-lower thermosphere region, relatively little is known about how WN4 impacts the ionosphere above the F-peak. We present an analysis of WN4 in the topside ionosphere at low latitudes as measured by the Defense Meteorological Satellite Program (DMSP) spacecraft. We investigate how the location and strength of WN4 in ion densities changes over two solar cycles and across local time and season, and interpret these variations in terms of composition and transport modified by the magnetic field geometry. Monthly averages of evening ion densities often clearly show a WN4 pattern along the magnetic equator which is strongest at equinox. In June solstice, WN4 moves 5-10o north, and ion densities are enhanced in regions of positive magnetic declination; in December solstice these effects are reversed. WN4 also moves slightly in latitude across the solar cycle, but this effect is much smaller than the seasonal effect. In general WN4 is strongly present in topside ion densities across all levels of solar activity and local times throughout the afternoon and evening.

COUP-14 - Solar impacts on atmospheric electric fields - by Greg Lucas

Status of First Author: Student IN poster competition, Masters

Authors: Greg Lucas, Jeff Thayer

Abstract: Vertical electric fields permeate our atmosphere due to a phenomenon known as the global electric circuit (GEC) that produces a global current system from the Earth's surface to the base of the ionosphere. Measurements of the near-surface electric field at low-latitude locations shows a good

correlation with global thunderstorm distributions [Whipple & Scrase 1941]. However, when one goes to high latitudes the ionosphere cross-cap potential is impressed upon the GEC modifying the near-surface vertical electric fields. [Lucas, et al. 2015] showed through a GEC simulation in WACCM that there are different locations where the solar wind driven cross-cap potentials will interact either in-phase or out-of-phase with the global electric circuit variations, producing different electric field signatures on the surface of the earth. The output from an array of electric field mills distributed across the Arctic and Antarctic will be presented to show how the ionospheric potential map can be determined through atmospheric electric field measurements.

Instruments or Techniques for Middle Atmosphere Observations

ITMA-01 - Inferring ratio of negative ion to electron concentration by using Arecibo Incoherent Scatter Radar - by Marcos Inonan

Status of First Author: Student IN poster competition, Undergraduate

Authors: John D. Sahr

Abstract: A new experiment has been implemented at Arecibo's Incoherent Scatter Radar to study D region parameters. This poster analyzes the width, amplitude and baseline of the ISR spectra to estimate the ratio of negative ion to electron concentration, which appear as the result of collisions between electrons and neutrals. Three models (Folded Lorentzian, folded Gaussian and folded Voigt functions) have been fitted to the data and the results was compared with the theoretical plasma parameters taken from the IRI model.

Additionally, an analysis of resulting ISR spectra has been made. Considering that the ISR spectra is obtained after a long incoherent integration, a combination of median/mean integration was applied in order to eliminate the outliers (echoes caused by airplanes or human interference) that could distort the spectra. This poster shows the best median/mean combination, after analyze the variance and SNR of the spectra.

ITMA-02 - Super Soaker: A Sounding Rocket Mission to Study Transport, Chemistry, and Energetics of Water in the Mesosphere and Lower Thermosphere and Implications for Polar Mesospheric Cloud Occurrence - by Irfan Azeem

Status of First Author: Non-student, PhD

Authors: Irfan Azeem, Rich Collins, Miguel Larsen, Mike Stevens, and Mike Taylor

Abstract: Water deposition in the Mesosphere and Lower Thermosphere (MLT) from space traffic (e.g. Meier et al., 2010) can lead to significant variations in the composition and dynamics of the region. The unexpectedly fast global-scale transport of the Space Shuttle's main engine exhaust can lead to the formation of polar mesospheric clouds (PMC) less than a day after launch [e.g. Stevens et al., 2003; Kelley et al., 2010]. This is an important finding because PMC have been implicated as possible indicators of long-term climate change [e.g. Thomas and Olivero, 2001 and references therein]. The formation of PMC from a low latitude launch raises a number of important questions about lower thermospheric and mesospheric processes, ranging from dynamics and chemistry to the integrity of the historical PMC record during the space age. The overall goal of the Super Soaker sounding rocket mission is to study the time-dependent neutral chemistry, energetics and transport of water in the MLT and to determine the resultant impact on the local temperature and PMC formation. The Super Soaker mission will include two sounding rockets launched from Poker Flat Rocket Range (PFRR), Alaska near 65° N. The first rocket will release trimethyl aluminum (TMA) trails and tracked optically to measure the background winds. The second rocket launched shortly after will release both TMA trails and disperse a large payload of water vapor in the MLT. The TMA trails will be tracked optically to measure any changes to the winds and to thereby

observe how the atmosphere responds dynamically to the injection of water. We will also observe the evolution of temperature and any ice particles in the MLT before, during and after the water release with lidar measurements from Poker Flat Research Range (PFRR). In addition, an Advanced Mesospheric Temperature Mapper (AMTM) instrument will be deployed to image the upper mesosphere (~87 km) before, during and after the water release to provide quantitative information on any dynamics/wave activity and changes in mesospheric temperature. Finally, we will continuously image the sky throughout the experiment at a variety of visible and IR wavelengths to quantify the formation and evolution of any mesospheric clouds formed as a result of the water release. The launch date is tentatively set for January 2018 to avoid the summertime PMC season over PFRR and ensure clear mesospheric air before the release. We will furthermore launch at twilight (solar depression angles between 8-16°) to optimize lighting for the lidar, AMTM, TMA and cloud images. Our ground-based observations will be supported by observations from the NASA TIMED satellite and numerical modeling results from the Thermosphere-Ionosphere-Mesosphere Energetics General Circulation Model (TIMEGCM). The Super Soaker sounding rocket mission, funded by the NASA Heliophysics Technology and Instrument Development for Science (H-TIDES) program, will deliver quantitative characterization of the thermodynamics, microphysics and chemistry of a concentrated parcel of water in the MLT region. To accomplish this goal the Super Soaker mission will: (a) assess whether the local environment is more or less conducive to PMC formation than an unperturbed atmosphere; (b) advance our understanding of the impact of space traffic on the upper atmospheric ice abundance, and; (c) develop key understanding of whether space traffic has contributed to the apparent secular increase of PMC occurrence over the past 50 years.

ITMA-03 - Spatial and Temporal Ionospheric Monitoring Using Broadband Sferics -
by Jackson C. McCormick

Status of First Author: Student IN poster competition, Masters

Authors: Jackson C McCormick
Morris B Cohen

Abstract: Very Low Frequency (VLF, 3-30kHz) radio waves are a useful diagnostic for lower ionospheric monitoring due to their reflection from this region and global propagation. Traditionally, the lower ionosphere has been sensed using single-frequency VLF transmitters allowing for analysis of a single propagation path, as there are only a small number of transmitters.

A lightning stroke releases an intense amount of impulsive broadband VLF radio energy in the form of a sferic, which propagates through the Earth-ionosphere waveguide. Lightning is globally distributed and very frequent, so a sferic is therefore also a useful diagnostic of the D-region. This is true both for ambient or quiet conditions, and for ionospheric perturbations such as solar flare x-ray bursts. Lightning strokes effectively act as separate VLF transmitting sources. As such, they uniquely provide the ability to add a spatial component to ionospheric remote sensing, in addition to their broadband signature which cannot be achieved with man-made transmitters. We discuss the broad coverage potential of sferic-based ionospheric monitoring.

ITMA-04 - INSPIRESat-1: Introduction and Feasibility Study for a CubeSat Mission for Middle and Upper Atmosphere Wind and Temperature Observations -
by Jih-Chin Lai

Status of First Author: Student NOT in poster competition, Masters

Authors: Loren Chang, Amal Chandran, Larry L. Gordley, David C. Fritts, Cornelius Csar Jude H. Salinas, Jack C. Wang, Jia-Yu Su, Joe Hong, Yi-chung Chiu, Cuan—Wen Chen, Pei—Yun Chiu, Duann Yi, Ya-Chih Mao, Pei-Ting Kao, Bing-Han Tsai, Tsung-En Tseng

Abstract: In terms of understanding on Earth's atmosphere, there are still numerous limitations due to the lack of global wind and temperature observations throughout the middle and upper atmosphere. The Doppler Wind and temperature Sounder (DWTS) is a cutting edge instrument that will be capable of

simultaneously measuring neutral winds and temperatures from the lower to the upper atmosphere (20-250km). In comparison to any other past or current instrument, the vertical coverage of DWTS is a tremendous breakthrough, which would contribute to improving current research and monitoring of atmospheric phenomena such as stratospheric dynamics, MLT/IT dynamical vertical coupling, as well as vertically-propagating tides and planetary waves from the lower to the upper atmosphere.

As a new instrument, DWTS still requires operational testing to raise its TRL, making it a possible candidate for a CubeSat mission. INSPIRESat-1 is a 6U CubeSat which is being co-developed by the University of Colorado Laboratory for Atmospheric and Space Physics (CU LASP), the Indian Institute for Space Science and Technology (IIST), and National Central University (NCU), with DWTS, built by GATS Inc. and Brandywine Photonics, as the mission payload. DWTS will use the modulated gas correlation technique with an infrared camera to measure Doppler shifts and widths of the nitric oxide emission spectrum to retrieve vertical profiles of neutral wind and temperature simultaneously. NCU will support this mission by designing and fabricating the engineering model of the INSPIRESat-1 satellite bus, as well as by supporting communications operations for data downlink and command uplink using a VHF/UHF ground station. Here we will highlight on the analysis, preliminary design, and requirements imposed on all the subsystems for the INSPIRESat-1 mission, as determined by our team of approximately 15 NCU graduate students. In addition, I will also present future work and milestones, which will strengthen the feasibility and capability of successful fabrication and function of this CubeSat mission.

ITMA-05 - Studies of Turbulence in the Arctic Mesosphere with PFISR - by Jintai Li

Status of First Author: Student NOT in poster competition, Masters

Authors: Jintai Li, Richard L. Collins, Cameron Martus, Michael Nicolls, Roger Varney and David E. Newman

Abstract: We present studies of turbulence in the Arctic mesosphere with Poker Flat Incoherent Scatter Radar (PFISR). We develop retrieval and analysis techniques to determine the characteristics of the turbulence and the nickel. We present measurements of mesospheric turbulence with PFISR on 23 April 2008 and 18 February 2013. We characterize mesospheric turbulence in terms of the energy dissipation rate as a function of altitude and time on these days. We present an extensive analysis of the radar measurements to show that the use of high quality PFISR data and accurate geophysical conditions are essential to achieve accurate turbulent measurements. We find that the retrieved values of the energy dissipation rate vary significantly based on data selection.

ITMA-06 - Thermospheric Temperature Analysis Methods for the OPAL Mission - by Preston Hooser

Status of First Author: Student IN poster competition, Undergraduate

Authors: Preston Hooser, Eric Ashby, Kenneth Zia, Ludger Scherliess, Mike Taylor, and the OPAL team

Abstract: The Optical Profiling of the Atmospheric Limb (OPAL) CubeSat mission is designed to measure the temperature in the thermosphere between 90 and 140 km. Temperatures will be inferred from the characteristic emission lines of molecular oxygen O₂ A-band (around 760 nm). These data will be used to better understand the effects of solar storms and atmospheric waves on the evolution of the temperature structure in this important region.

The steps to retrieve the temperature from the relative spectral photon flux measurements made by OPAL, as well as the deconvolution of the data, will be discussed. Initial results, using synthetic data, of the temperature recognition and inversion algorithms are presented. These methods are then applied to a modeled OPAL measurement to estimate the uncertainties in temperature measurements made by the instrument on orbit.

ITMA-07 - Proposing an upgrade of the Arecibo lidar systems to enhance science capabilities - by Jens Lautenbach

Status of First Author: Non-student, PhD

Authors: J. Lautenbach, S. Raizada, E. Franco, J. S. Friedman

Abstract: To enhance the science capabilities of the Arecibo lidar systems we propose I: upgrade the current potassium lidar to an iron lidar. This upgrade will achieve high-resolution wind and temperature measurements in the upper atmosphere and improving our current temperature range & time resolution by a factor of 5. Fe is highly favorable for lidar observations because its density is ~200 times higher than K. With recent observations of metal atoms at altitudes up to 150 km we anticipate that observations of Fe will enhance our ability to study the neutral component of the thermosphere. This enables closer collaboration with Incoherent Scatter Radar (ISR) studies of the thermospheric plasma, providing an excellent opportunity to investigate characteristics of the Fe layer in conjunction with Sporadic E layers - Fe⁺ being a major constituent of Es. There is a particular opportunity at Arecibo, with its multiple resonance lidars, ISR and other observing platforms, to comprehend daily variability. In addition, multiple resonance lidars at Arecibo allow us to shed light on distribution of alkali and non-alkali metals. II: upgrade the current Rayleigh lidar to obtain whole atmospheric temperature profiles. Combined Rayleigh and Resonance Doppler temperatures will allow us to investigate the coupling between different atmospheric regions, and in particular we can study the influence of Stratospheric warming events on the upper atmospheric region along with wave coupling. Additionally, the impact of space weather events can be explored by such unique instrumentation at Arecibo.

Long Term Variations of the Mesosphere and Lower Thermosphere

LTVM-01 - Intermittency of Gravity Waves Momentum Flux in Airglow Imager Observations and Whole Atmosphere Community Climate Model (WACCM) - by Bing Cao

Status of First Author: Student IN poster competition PhD

Authors: Bing Cao, Alan Z. Liu

Abstract: Gravity waves with specific properties will not generally be occurring throughout the entire area and time, factors that can describe the spatial and/or temporal intermittency of should be considered in the Global Circulation Models (GCMs). In this work, observation data from an all-sky airglow imager is used to analyze the intermittent nature of gravity waves near mesopause region. The probability density functions (pdfs) of gravity wave momentum flux show that they largely follow a log-normal distribution; at the tail for larger magnitudes, they deviate from the log-normal distribution and follow a power-law distribution. Also, multi-year simulation results from Whole Atmosphere Community Climate Model with Specified Dynamics (SD-WACCM) are used to analyze the gravity wave intermittency. The gravity waves momentum flux and forcing data is generated hourly in global range. By analyzing the pdfs of the model data, the geographical, altitude and seasonal variations of intermittency are discussed and compared with the results from the observation data.

LTVM-02 - An analysis of long-term trends in mesospheric temperatures from OH airglow spectra of Kiruna FTS and Sloan Digital Sky Survey - by Gawon Kim

Status of First Author: Student IN poster competition, Masters

Authors: Gawon Kim, Yong Ha Kim, Youngsun Lee, Jeong-Han Kim

Abstract: We have analyzed mesospheric temperatures from OH airglow measurements with Fourier Transform Spectrometer (FTS) in the period of 2003 – 2012 at Kiruna (67.9N, 21.1E). We also derived mesospheric temperatures from rotational emission lines of the OH airglow (8-3) band in the sky spectra of Sloan Digital Sky Survey (SDSS), which were measured at Apache Point Observatory (APO, 32°N 105°W) in the period of 2000 – 2014. We have found the seasonal variations, solar responses and long-term variations of mesospheric temperatures at both sites. FTS temperatures show signals of sudden stratospheric warming (SSW). The solar responses are $5.0\text{K}\pm 1.5\text{K} / 100\text{SFU}$ in FTS temperatures and $1.7\text{K}\pm 0.8\text{K} / 100\text{SFU}$ in SDSS temperatures. After removing the solar responses, the long-term trends are found to be $-2.6\text{K}\pm 1.5$ and $-1.0\text{K}\pm 0.9\text{K}/\text{Decade}$ over Kiruna and Apache Point, respectively. Our results indicate significant cooling trend at the high latitude but very little or no cooling at the low latitude. Although both trends are comparable and consistent with other studies, the temperature trend from SDSS spectra should be regarded as unique contribution to global monitoring of climate change because the SDSS project is completely independent of climate studies. Finally we discuss our results by comparing with those of Microwave Limb Sounder (MLS) instrument on board Aura satellite.

Meteor Science other than wind observations

METR-01 - Radio-Frequency Emissions from Hypervelocity Meteoroid Impacts –

by Andrew Nuttall

Status of First Author: Student IN poster competition, Masters

Authors: Andrew Nuttall, Sigrid Close

Abstract: Spacecraft face many unique hazards when operating in the space environment. Over the last 50 years, as our knowledge of the space environment has increased, many of these hazards have been able to be mitigated through intelligent satellite and mission design. However, a significant portion of satellite failures still cannot be attributed to our current understanding of the space environment. One uncharacterized hazard comes from the frequent collisions between high velocity dust sized meteoroids and satellites. These collisions have the potential to generate unwanted electrical effects through the impact generated plasma. One potential hazard that can be generated through this mechanism is wideband electromagnetic pulses in the radio-frequency (RF) spectrum. High power RF emissions can induce damaging currents in sensitive electronics and can create disturbances in nominal sensor behavior and performance. To investigate this phenomena, ground-based tests were conducted at dust accelerator and light gas gun facilities. Impact cases were run with varying bias voltages on the target to recreate the natural spacecraft charging conditions that can occur in orbit. Wideband RF emissions were observed under multiple different spacecraft charging conditions. An initial scaling analysis suggests that the peak power of these RF emissions can reach hazardous levels for large mass and velocity dust sized impacts.

METR-02 - Spectra of Full 3-D PIC Simulations of Turbulent Meteor Trails -

by Liane Kathryn Tarnecki

Status of First Author: Student NOT in poster competition, Undergraduate

Authors: Liane Tarnecki, Meers Oppenheim

Abstract: Radars detect plasma trails created by the billions of small meteors that impact the Earth's atmosphere daily, returning data used to infer characteristics of the meteoroid population and upper atmosphere. Researchers use models to investigate the composition and evolution of the meteors and plasma trails. In this paper, we examine spectra from full 3D simulations of meteor trail evolution under a variety of conditions, including a range of external electric fields and collision rates. The results of this study will allow more detailed and accurate information about the meteors to be drawn from non-specular radar observations of the trails, and aid in identifying the characteristics of the meteors that are best described by the simulations.

METR-03 - Particle In Cell Simulation of Meteor Head Echo - by Glenn Sugar

Status of First Author: Student IN poster competition, PhD

Authors: Glenn Sugar, Siddarth Krishamoorthy, Sigrid Close

Abstract: As a meteoroid ablates in the ionosphere, layer of plasma is generated with a density orders of magnitude higher than the background ionospheric plasma density. High power large aperture radars frequently detect this plasma as meteor head echoes. In order to determine the mass of the parent meteoroid, it is important to understand the characteristics of the plasma that causes the head echo. Current models used for calculating meteoroid mass from radar observations must assume a plasma density distribution around the meteoroid. However, the assumed density distributions are based on simplified models that have not been experimentally verified. In order to test whether these assumptions are valid, we ran 2D electrostatic particle-in-cell (PIC) simulations using PICard, a PIC simulator developed by the Space Environment and Satellite Systems lab at Stanford University. We present results from meteoroids ablating both with and without fragmentation, and compare the simulation results to models used for determining meteoroid mass from head echo observations.

METR-04 - Effect of Plasma Turbulence on the evolution of Specular Meteor Echoes - by Freddy Ronald Galindo

Status of First Author: Student IN poster competition, PhD

Authors: F. R. Galindo¹, J. V. Urbina¹, L. P. Dyrud² and J. Fentzke²

(1) Communications and Space, Sciences Laboratory, Pennsylvania State University, University Park, PA
(2) OmniEarth, Inc. 2015. 251 18th Street South - Suite 650, Arlington VA 22202

Abstract: Specular meteor echoes are signals back-scattered from expanding trails of ionized particles created during the passage of a meteoroid through the upper atmosphere, when a radar k vector points perpendicularly to the trajectory of the trail. These radar echoes are currently used to derive atmospheric parameters such as temperature, pressure, and drifts; under the assumption of non-turbulent diffusion rate. In this paper, we describe a numerical model of under-dense specular meteor echoes that includes for the first time the effect of plasma turbulence on its evolution. Our numerical method simulates both the trail at different stages and its corresponding received power. This numerical model can easily be expanded to include physical processes (e.g. differential ablation) that briefly affect the evolution of the specular meteor echo.

We present the analysis of a specular meteor echo that exhibit a double decay as a case study. Our simulations demonstrate that meteor events similar to this double decay can occur when time-scales to produce plasma turbulence in the trail is on the order of hundreds of milliseconds, or when plasma turbulence ceases rapidly. Furthermore, we report meteor simulation results in conjunction with specular meteors collected with the Chile Meteor Radar. These simulations incorporate the studies of diffusion values, which are modeled by including/excluding the effect of the Earth's geomagnetic field and plasma turbulence. Upon examination of simulations and experimental data, our preliminary studies illustrate the significant effect that turbulence plays on the evolution of underdense specular meteor echoes. This result is particularly useful to infer more accurate mesospheric temperatures from trail diffusion rates and their usage for meteor scatter communication systems.

METR-05 - Size Distribution Of Fragmented Grains From The Intensity And Duration Of Meteor Flares - by Diana Juarez Madera

Status of First Author: Student NOT in poster competition, PhD

Authors: Diana Juarez Madera, Sigrid Close, William Cooke and Danielle Moser

Abstract: The meteor phenomenon is produced by ablation or mass loss from the surface of the meteoroid through intense heating. The sudden bursts or flares observed along the visual path of a meteor are likely related to the increase of the mass loss rate during the flight. The extra light is assumed to be produced by the complete fragmentation of the body, leading to the simultaneous detachment of smaller particles or grains. By measuring the intensity and duration of flares observed with a wide-field camera capturing at 110 frames per second, the size distribution of the grains was obtained through flare fitting. The grain size lies within 15-500 micrometers and the mass distribution index from -1.1 to -3.5.

METR-06 - Detection and Characterization of Meteoroid From Optical and Radar Observations - by Lorenzo Limonta

Status of First Author: Student IN poster competition, Masters

Authors: Sigrid Close, Robert Marshall

Abstract: Optical and radar mass determinations are fraught with error due to difficulty in assessing the luminous efficiency τ (for optical) and the ionization probability β (for radar) parameters, both of which depend on the meteor velocity and composition, as well as surrounding air density. In order to investigate the relationship between these two coefficients, we conducted one of the few dual-observation experiment of meteoroid in the optical and radar spectrum. Thanks to the accuracy of the equipment at our disposal during our stay at the Poker Flat Research Range, we were able to detect such events at a higher rate than previous experiments. Our analysis revealed two key findings: the differential ablation in radar data suggested by Janches [1] seems to be confirmed by the corresponding optical signal. Additionally, our investigation on the relationship between τ and β suggests that among the existing choices of coefficients, Jones 1997 [2] and Hill 2005 [3], give the more precise — thou not necessarily accurate — results.

MLT Gravity Waves

MLTG-01 - Investigating Seasonal Mesospheric Gravity Wave Propagation and Variability - by Ahmad Talaei

Status of First Author: Student IN poster competition, Masters

Authors: Ahmad Talaei, Mike Taylor and Pierre-Dominique Pautet

Abstract: In this work, we analyze and evaluate seasonal phase speed distribution of mesospheric gravity waves over South Pole, Antarctica. This is a unique data set that has been obtained over the past four years using a new instrument designed at USU. The goal is to investigate for the first time the variability of gravity waves during the course of winter season and subsequent season to season variability over the four year data set. The gravity waves transfer the large amount of momentum into the atmosphere and investigating the seasonal and year to year variability will provide the novel measure of Antarctica.

MLTG-02 - DEEPWAVE: Ground-based analysis of Mesospheric Gravity Wave Signatures - by Pattilyn Frances McLaughlin

Status of First Author: Student NOT in poster competition, PhD

Authors: Pattilyn McLaughlin

Abstract: DEEPWAVE, or the Deep Propagating Gravity Wave Experiment is a four-year comprehensive measurement and modelling program designed to characterize and predict the generation and propagation of deeply propagating atmospheric waves with measurements extending from the ground to ~100 km

altitude. These waves typically arise from sources located at lower altitudes such as storms, frontal weather systems and mountain ranges, and then dissipate at high altitudes in the mesosphere and lower thermosphere (>80 km altitude) depositing large amounts of momentum into the upper atmosphere with regional and global impacts on the wind and temperature field. This is an international program involving a broad suite of aircraft borne and ground based aeronomic and weather measurements in conjunction with available satellite and high-resolution modelling predictions. New Zealand was chosen as it has been previously identified as a “hot spot” for gravity wave activity in the stratosphere using several satellite studies, however little was known if this region of activity extended to higher altitudes with strong wave penetration into the overlying mesosphere and thermosphere. During this campaign, two Advanced Mesospheric Temperature Mappers (AMTM) were used to measure the horizontal gravity wave temperature structures in the OH airglow emission (at ~87km) to quantify the wave field characteristics, amplitudes and to help identify the dominant sources over New Zealand. One AMTM was deployed on the Gulfstream V aircraft, while a second AMTM was set up and operated automatically from Lauder, New Zealand. This poster will give an overview of the DEEPWAVE Campaign and discuss a detailed analysis of the first night of gravity wave image data obtained by the Lauder-based AMTM.

MLTG-03 - Synthetic Airglow All-Sky Imager Data for the Interpretation of Gravity Waves Imaged Over Wide Fields of View - by Jaime Aguilar

Status of First Author: Student IN poster competition, PhD

Authors: Jonathan B. Snively, Alan Z. Liu

Abstract: All-sky airglow imagers are now frequently used for observing and analyzing gravity wave processes. This imager data provides the clearest insight into processes centered on its zenith. At large fields-of-view (FOVs) there is an expected decrease in spatial resolution but also significant line-of-sight (LOS) effects as the integration path lengths extend deeply and obliquely through the perturbed airglow emission layers. In order to more accurately interpret these off-zenith observations, a better understanding of the LOS effects is needed. The integration of the vertical emission rates represents loss of information regarding the structure of the airglow layer as it effectively “flattens” it. While this process is non-invertible with real airglow data, the use of simulated airglow structures enables direct comparisons with the structures present within the emitting layers. Here we present an investigation of simulated 2D and 3D airglow images as compared to the modeled airglow layer structures and corresponding synthetic ground-based zenith-integrated imager data. A fully nonlinear, compressible, 2D and 3D model [e.g., Snively et al., 2010] is used to generate distinct wave packets that are then integrated along the LOSs of simulated CCD pixels and an 180° FOV all-sky lens. An analysis of the filtering of scales, asymmetry of the integrated signals (indicated by the “Venetian Blind” effect), cancellation and apparent steepening effects are discussed for large FOVs for different wave phenomena. Specifically, we consider small scale waves perturbing different parts of the OH layer and large amplitude nonlinear wave processes. Comparisons are made between the vertical integration (in geographic coordinates) to the LOS integration as seen by the synthetic all-sky imager (unwarped from airglow-imager geometry), to provide guidance for the interpretation of small-scale gravity waves and wave processes imaged off-zenith.

MLTG-04 - Modeling of mountain-generated gravity waves - by Thomas Lobay

Status of First Author: Student IN poster competition, Undergraduate

Authors: Thomas Lobay, Andrew Gerrard, Gil Jeffer, Anthony Teti

Abstract: Molecular/aerosol lidar measurements taken from NJIT-CSTR’s Jeffer Observatory in Hope, NJ show an often replicated gravity wave feature in relative density measurements of the upper troposphere and stratosphere. This gravity wave pattern demonstrates phase variation in altitude, unlike traditional stationary wave phase patterns associated with mountain-generated gravity waves. Herein we present

modeling efforts to describe and characterize this wave morphology. We demonstrate that the generation of secondary gravity waves, caused by the persistent breaking of mountain-generated waves from the Appalachian Plateau Regions, is the likely cause.

MLTG-05 - Mesospheric Gravity Waves and their Sources at the South Pole -
by Dhvanit Mehta

Status of First Author: Student IN poster competition, PhD

Authors: Dhvanit Mehta, Andrew J. Gerrard, Yusuke Ebihara, Allan T. Weatherwax, Louis J. Lanzerotti

Abstract: The sourcing locations and mechanisms for short period, long vertical wavelength upward-propagating gravity waves at high polar latitudes remain largely unknown. Using all-sky imager data from the Amundsen-Scott South Pole Station we determine the spatial and temporal characteristics of 94 observed small-scale waves in three austral winter months in 2003 and 2004. These data, together with background atmospheres from synoptic and/or climatological empirical models, are used to model gravity wave propagation from the polar mesosphere to each wave's source using a ray-tracing model. Our results provide a compelling case that a significant proportion of the observed waves are launched in several discrete layers in the tropopause and/or stratosphere. Analyses of synoptic geopotentials and temperatures indicate that wave formation is a result of baroclinic instability processes in the stratosphere and the interaction of planetary waves with the background wind fields in the tropopause. These results are significant for defining the influences of the polar vortex on the production of these small-scale, upward propagating gravity waves at the highest polar latitudes.

MLTG-06 - Modeling atmospheric gravity waves using the Transfer Function Model (TFM) and the associated ionospheric responses - by Robert Bruntz

Status of First Author: Non-student, PhD

Authors: Robert Bruntz, Hans Mayr, Larry Paxton, Ethan Miller, Gary Bust.

Abstract: The Transfer Function Model (TFM) is a linear model that solves the equations for the conservation of mass, energy, and momentum in the atmosphere, from 0 to 700 km, for 5 species (N₂, O, H, He, Ar) and 4 parameters for each (density + 3 components of velocity), plus the (same) temperature for all species. TFM is unusual in that rather than solving the equations and obtaining results on a fixed grid, the response to a delta-function source is saved in an intermediate-state transfer function, which can be combined with any number of different sources in a separate step, producing the atmospheric response on a user-defined grid of arbitrary resolution in time or colatitude. The model uses zonally-symmetric sources (cylinders at the pole or pole-centered rings), which can then be linearly combined to simulate complicated sources. We will present results of recent investigations using the TFM to explore gravity waves from a variety of sources and the associated ionospheric responses.

MLTG-07 - Two-dimensional Morlet wavelet transform and its application to extracting two-dimensional wave packets from lidar observations in Antarctica -
by Cao Chen

Status of First Author: Student IN poster competition, PhD

Authors: Xinzhao Chu

Abstract: Persistent, dominant, and large-amplitude gravity waves with 3–10h periods and vertical wavelengths ~20–30km are observed in temperatures from the stratosphere to lower thermosphere with an Fe Boltzmann lidar at McMurdo, Antarctica. These waves exhibit characteristics of inertia-gravity waves in case studies, yet they are extremely persistent and have been present during every lidar observation. We

characterize these 3–10h waves in the mesosphere and lower thermosphere using lidar temperature data in June from 2011 to 2015. A new method is applied to identify the major wave events from every lidar run longer than 12 h. A continuous 65 h lidar run on 28–30 June 2014 exhibits a 7.5 h wave spanning ~60 h, and 6.5h and 3.4h waves spanning 40 and 45 h, respectively. Over the course of 5 years, 323h of data in June reveal that the major wave periods occur in several groups centered from ~3.5 to 7.5 h, with vertical phase speeds of 0.8–2 m/s. These 3–10 h waves possess more than half of the spectral energy for ~93% of the time. A rigorous prewhitening, postcoloring technique is introduced for frequency power spectra investigation.

The resulting spectral slopes are unusually steep (2.7) below ~100km but gradually become shallower with increasing altitude, reaching about 1.6 at 110 km. Two-dimensional fast Fourier transform spectra confirm that these waves have a uniform dominant vertical wavelength of 20–30km across periods of 3.5–10 h. These statistical features shed light on the wave source and pave the way for future research.

1.

MLTG-08 - Gravity Wave Instability Evolution in Variable Stratification and Shear - by Tyler Mixa

Status of First Author: Student IN poster competition, Masters

Authors: Tyler Mixa, Dave Fritts, Brian Laughman, Ling Wang, and Lakshmi Kantha

Abstract: An anelastic numerical model is used to investigate the evolution of gravity wave instability dynamics in mesospheric stratification and shear environments. Recent computational advances allow the characterization of localized gravity wave packets in a deep, dynamic atmosphere, enabling realistic amplitude evolution and sensitivity to transient nonlinear dynamics. Gravity wave self-acceleration alters the wave amplitude and enhances the local mean flow as the packet propagates, driving stably-stratified structures to instability where the wave packet impinges on sheets and layers. The results reveal that gravity wave and mean shears combine to evolve Kelvin-Helmholtz instabilities (KHI) on sheets of high stratification where GW vertical displacements approach their maxima. The KHI arise at smaller scales and grow with time, as seen in lidar, radar, and airglow observations. Such highly localized events are a major mechanism driving turbulence and mixing in the MLT, and these simulations enable their characterization at scales that are challenging to resolve with existing measurement capabilities.

MLTG-09 - First Observations from the February 2016 World Day on Gravity Waves - by Andrew J. Kavanagh

Status of First Author: Non-student, PhD

Authors: Andrew J. Kavanagh

Abstract: Gravity waves are recognized as an important mechanism for transporting momentum from the lower atmosphere into the mesosphere and driving the meridional pole to pole circulation. Modelling and observations have shown that waves are capable of penetrating higher into the thermosphere, either directly or via the generation of secondary waves as the initial waves break. Gravity waves in the thermosphere interact with the ionized atmosphere causing Travelling ionospheric disturbances (TID). TID can also be generated insitu by processes such as Joule Heating and it is still yet to be determined which is the dominant mechanism of TID generation and whether we can see the gravity waves playing an important role in the variability of the thermosphere. In February 2016 the Incoherent Scatter Radars operated in conjunction for 5 days as part of a World Day. The period was quite disturbed, both in terms of geomagnetic activity and lower atmosphere forcing. I will present initial data from the period and highlight interesting features with TID characteristics.

MLTG-10 - Comparison of gravity wave induced airglow variations using MSIS-90 and NRLMSISE-00 atmospheric density models - by Yolian Amaro-Rivera

Status of First Author: Student NOT in poster competition, PhD

Authors: Yolian Amaro-Rivera, Tai-Yin Huang, Julio Urbina

Abstract: We employ two 2-dimensional, nonlinear, time-dependent numerical models, Multiple Airglow Chemistry Dynamics (MACD) and OH Chemistry Dynamics (OHCD), to investigate gravity wave induced airglow variations in the Mesosphere and Lower Thermosphere (MLT) region. Our work is focused on the OH airglow, O₂(0,1) atmospheric band, and O(1S) greenline airglow emissions. The atmospheric reference model has been upgraded from MSIS-90 to NRLMSISE-00. One of the reasons for upgrading to NRLMSISE-00 is that the model contains recent data on temperature and molecular oxygen number density, O₂. Also, the techniques used to process incoherent scatter radar data have experienced significant changes since 1990, which leads to superior quality of the inferred ionospheric properties. We will report the changes on minor and major gas densities, as well as the temperature retrieved from both reference models, and investigate how this affects the aforementioned airglow emissions.

MLT Lidar Studies

MLTL-01 - Obtaining Continuous Observations from the Upper Stratosphere to the Lower Thermosphere Using the ALO-USU Rayleigh-Scatter Lidar - by Jonathan Price

Status of First Author: Student IN poster competition, PhD

Authors: Jonathan Price, Vincent Wickwar, Leda Sox, Mathew Emerick, Josh Herron, Shayli Elliott, Bryant Ward, Benjamin Lovelady

Abstract: The Rayleigh-scatter lidar at the Atmospheric Lidar Observatory at Utah State University (ALO-USU; 41.74° N, 111.81° W) started observations in 1993. In 2012 the original lidar system was upgraded with an array of larger mirrors and two lasers to enable observations of the upper mesosphere and lower thermosphere from 70 km to about 115 km in altitude. (Continued refinement should provide data to above 120 km.) Recently, the original system was reconfigured [Elliott, et al., 2016] to again observe the lower mesosphere between 40 km and 90 km. Initial data collected by these two parts of the Rayleigh system have been “stitched” together to obtain full signal profiles from 40 km to about 115 km. These extended profiles have been used to obtain relative neutral density and temperature profiles through the entire mesosphere and well into the lower thermosphere. This extends the CEDAR goal of studying coupling between atmospheric regions. Furthermore, by normalizing the relative neutral densities between 40 and 45 km to an advanced reanalysis model, absolute neutral densities become available from a ground-based, remote-sensing instrument all the way into the lower thermosphere. This opens that region to detailed study and provides the ability to examine the lower boundary conditions for thermospheric models.

MLTL-02 - Simultaneous, collocated Rayleigh and sodium lidar temperature comparison - by Leda Sox

Status of First Author: Student IN poster competition, PhD

Authors: Leda Sox, Vincent B. Wickwar, Tao Yuan, Neal R. Criddle

Abstract: There are relatively few instruments that have the capabilities to make near continuous measurements of the mesosphere-lower-thermosphere (MLT) region. Rayleigh-scatter and resonance lidars, particularly sodium (Na) resonance lidar, have been the two dominant ground-based techniques for acquiring mesosphere and MLT vertical temperature profiles, respectively, for more than two decades.

With these measurements, the dynamics and long-term temperature trends of the MLT region can be studied. For the first time, we will present simultaneous, night-time averaged temperatures acquired from the same observational site, on the campus of Utah State University (USU), using these two lidar techniques. This comparison is also unique in that this will be the first time that the Rayleigh and Na lidar profiles will cover the same altitude range (80-110 km). This altitude overlap has been achieved through upgrades to the existing USU Rayleigh lidar, which elevated its observational range from 45-90 km to 70-115 km, making it one of two Rayleigh lidars in the world that can extend into the thermosphere, and by the relocation of the Colorado State Na lidar to the USU campus. The comparison of the two sets of temperature measurements is important because the two lidar techniques derive temperature profiles using different observational techniques and analysis methods, each of which are based on different sets of physical assumptions and theories. Furthermore, previous climatological comparisons between Rayleigh and Na lidar, in the 80-90 km range, have suggested that significant temperature differences can occur. This comparison aims to extend the climatological studies by exploring the agreement between the lidar techniques' temperatures with respect to altitude and season.

MLTL-03 - Seasonal Temperatures from the Upper Mesosphere to the Lower Thermosphere Obtained with the Large, ALO-USU Rayleigh Lidar -
by Vincent B. Wickwar

Status of First Author: Non-student, PhD

Authors: Vincent B. Wickwar, Leda Sox, Matthew T. Emerick, Joshua P. Herron

Abstract: Observations have been made with the large, Rayleigh-scatter lidar at the Atmospheric Lidar Observatory at Utah State University (ALO-USU; 41.74° N, 111.81° W) from summer 2014 to summer 2015. During this first operational year, the lidar acquired nearly 100 nights of observations between 70 and 115 km altitude, i.e., from the upper mesosphere, through the mesopause, and into the lower thermosphere. This was possible because of the large 4.9 m² collecting area of the mirrors and the 42 W of emitted power at 532 nm at a 30 Hz emission rate. These two factors produce a figure of merit, a power-aperture-product, of 205 Wm², making this one of the two most sensitive Rayleigh lidars in the world. The all-night data have been reduced to obtain relative densities and absolute temperatures. The temperatures are divided into three-month intervals, which are used to determine variations in altitude and in time. They clearly show significant and complex patterns. Additionally, they are compared to the original ALO-USU temperature climatology, which extends from 45 to 90 km, from 11 years of data from the original lidar, and they are compared to the temperatures from the NRL-MSISE00 empirical model.

MLTL-04 - Reestablishing Observations throughout the Mesosphere with the ALO-USU Rayleigh-Scatter Lidar - by Shayli Elliott

Status of First Author: Student IN poster competition, Undergraduate

Authors: Elliott, Shayli, Bryant Ward, Benjamin Lovelady, Jessica Gardner, Lucas Priskos, Matthew T. Emerick, and Vincent B. Wickwar

Abstract: In the last few years, the Rayleigh-scatter lidar at the Atmospheric Lidar Observatory at Utah State University (ALO-USU; 41.74° N, 111.81° W) has been upgraded to extend observations from 70 km up to 115 km. This project describes a student project to build and use a complementary Rayleigh-scatter lidar to go from 40 to 90 km, from the upper stratosphere to the upper mesosphere. At the upper end, this new lidar overlaps with the high-altitude lidar. This was done in a period of just over two months. This lidar shares the same lasers, but introduces a 44-cm mirror and a new telescope for the lower altitude observations. The rest of the detector chain is modelled after the one used in the larger lidar. This small lidar will provide a ground-based way of remote sensing the upper stratosphere and mesosphere. Combined with the existing larger lidar, the entire system, covering 40 to 115 km, will provide continuous observations well up into the lower thermosphere. This combined system gives the greatest coverage of any Rayleigh lidar in the world.

MLTL-05 - Searching for Troposphere-Mesosphere Connections Using the USU Rayleigh Lidar - by David K. Moser

Status of First Author: Student IN poster competition, Masters

Authors: David K. Moser, Vincent B. Wickwar, Joshua P. Herron

Abstract: The paucity of whole-atmosphere data introduces significant challenges that hinder the study of atmospheric couplings. The mesosphere in particular is a low-information void between the lower and upper atmosphere, which may prevent us from a complete realization of vertical interactions. The Rayleigh-scatter lidar at Utah State University's Atmospheric Lidar Observatory (ALO-USU; 41.74° N, 111.81° W) operated with little interruption from 1993 to 2004, providing a valuable temporal and spatial (45 – 90 km) resource in this realm. When studied alongside a multitude of other atmospheric data sources, possible unforeseen connections or insights may result. In this study, an adaptive fit is applied to near-stratopause temperature data from the lidar and several assimilative models to identify simultaneous abnormal changes. A possible connection with tropospheric events is investigated as an example of future efforts that can be made to synthesize similar environmental figures where available.

MLTL-06 - Characterization of gravity waves in the stratosphere and lower mesosphere at McMurdo, Antarctica - by Jian Zhao

Status of First Author: Student IN poster competition, PhD

Authors: Jian Zhao, Xinzhao Chu, Cao Chen, Xian Lu, Weichun Fong, Brendan R. Roberts, Zhibin Yu, and John A. Smith

Abstract: Five years' data has been accumulated since University of Colorado Lidar group deployed an Fe Boltzmann Lidar at McMurdo Station, Antarctica. This study characterizes the vertical wavelength, period, phase speed, occurrence rate/time, and potential energy density of gravity waves in the Rayleigh temperature region over the five years. A close correlation between potential energy density and background wind was also revealed.

MLTL-07 - First results from new observational capabilities of the Na Lidar at Utah State University - by Luis Navarro

Status of First Author: Student NOT in poster competition, PhD

Authors: Luis Navarro, Titus Yuan

Abstract: The Sodium Lidar at Utah State University (41°44'33''N, 111°48'29''W) was first developed and deployed at Colorado State University at 1989. Since then it has gone through several critical upgrades to extend its measurement capabilities. It has served to monitor the sodium metal layer in the mesosphere through measuring Na density, winds and temperature not only at nighttime but also during daytime. It has gather enough data to calculate the climatology on the mesopause region temperature among other studies.

Recently, the lidar receiver has been updated to allow 4-channel operation that allows the measurements of gravity wave momentum flux in both zonal and meridional directions within the mesopause region. We are presenting the first results through this upgrade, which will advance the understanding of gravity wave forcing in the mesopause region.

MLTL-08 - Latitudinal variations on winds and temperature between ALO and USU Na Lidars - by Luis Navarro

Status of First Author: Student IN poster competition, PhD

Authors: Luis Navarro, Titus Yuan, Fabio Vargas, Gary Swenson

Abstract: Global measurements of neutral winds and temperatures of the mesosphere and lower thermosphere are important to understand different phenomena and altitude-dependent perturbations.

Among the instrumentation available to reach this goal, the Sodium Lidars at Utah State University (41°44'33''N, 111°48'29''W) and at the Andes Lidar Observatory (30°10'43''S, 70°48'9''W) are continuously monitoring these space weather parameters for a better understanding of different phenomena

Being both part of the Consortium of Resonance and Rayleigh Lidars (CRRL), the data gathered by these instruments from several campaign runs are being compared starting in February and March 2016 when both lidars were running simultaneously. This data are used to investigate the day-to-day and latitudinal variations, as well as the comparative Na density at different longitudinal sectors illustrating interesting findings.

MLTL-09 - Variations in mesospheric densities from Rayleigh lidar observations at Golmud - by Shuai Qiao

Status of First Author: Student IN poster competition, PhD

Authors: Shuai Qiao; Weilin Pan

Abstract: As the Earth's third pole, the Tibetan Plateau has a significant influence on global climate especially the Asian monsoons. A Rayleigh lidar at Golmud station (36.25°N, 94.54°E), Qinghai, measured density profiles and variations from 50 to 90 km between September 2013 and October 2015 over Tibetan plateau. Annual mean lidar density profile was agree well with MSIS-00 model prediction in the region of 55-65 km, but lower than Mass Spectrometer and Incoherent Scatter (MSIS-00) model from 65 to 98 km. Both lidar results and model prediction show significant annual and semiannual variations of density in mesosphere.

MLTL-10 – Statistical characterization of high-to-medium frequency gravity waves in vertical winds and temperatures measured by lidar in the MLT – by Xian Lu

Status of First Author: Non-student, PhD

Authors: Haoyu Li, Xinzhao Chu, Cao Chen

Abstract: Due to the significant improvement of the receiver efficiency of the STAR lidar at Boulder, the vertical winds can now be directly measured with high temporal and spatial resolutions. The most dominant wave signatures in vertical winds are those with periods of 0.5-2.5 h. Using 1-year of vertical wind and temperature data, we derive the probability density functions of wave amplitudes and the amplitude ratios of temperature versus vertical wind, phase differences between these two components, vertical wavelengths, and heat fluxes induced by these GWs. It is found that the longer period waves tend to have larger amplitudes in temperature and smaller ones in vertical wind, while the phase difference between temperature and vertical wind largely follows a Gaussian distribution with a mean at ~90 degree. The means of the amplitude ratio and phase difference support the polarization relation of GWs between temperature and vertical wind, while the standard deviations may represent the effects from wave dissipations. The quasi-symmetric distribution of phase difference centered around 90 deg implies that dissipation or saturation process of GW can cause both positive and negative heat flux for a single wave locally. The distribution of phase difference around 90 deg leads to small heat fluxes, implying that the contribution from this spectrum of GWs may not be significant in terms of heat budget. The lognormal distribution of heat flux is also identified, i.e., larger heat flux events occur rarer, but can make significant contribution to the total flux. This feature is consistent with previous studies on the intermittency of GWs which shows similar lognormal distributions of wave variances, momentum flux and potential energy. The

gravity waves studied in this paper fall into the mesoscale wave range, which have not been resolved in the GCMs until recently by the high-resolution GCMs. Therefore, the statistical results of various wave characteristics and heat fluxes provide an invaluable validation basis for high-resolution GCMs and the fine-resolution weather models.

MLTL-11 - Gravity Wave and Turbulence Transport of Heat and Na in the Mesopause Region over the Andes - by Yafang Guo

Status of First Author: Student IN poster competition, PhD

Authors: Alan Z. Liu, Chester S. Gardner

Abstract: The vertical heat and Na fluxes induced by gravity waves and turbulence are derived based on over 600 hours of observations from the Na wind/temperature lidar located at Andes lidar Observatory (ALO), Cerro Pachón, Chile. In the 85-100 km region, the annual mean vertical fluxes by gravity waves show downward heat transport with a maximum of 0.78K m/s at 90 km, and downward Na transport with a maximum of 210 m/s/cm³ at 94km. The maximum cooling rate reaches -24 K/d at 94km. The vertical fluxes have strong seasonal variations, with large differences in magnitudes and altitudes of maximum fluxes between winter and summer.

The vertical fluxes due to turbulence eddies are also derived with a novel method that relates turbulence fluctuations of temperature and vertical wind with photon count fluctuations at very high resolution (25 m, 6 s). The results show that the vertical transports are comparable to those by gravity waves and they both play significant roles in the atmospheric thermal structure and constituent distribution. This direct measure of turbulence transport also enables the estimate of the eddy diffusivity for heat and constituent in the mesopause region.

MLTL-12 - Lidar observation of thermosphere sodium layers at Andes Lidar Observatory (30.25° S, 70.74° W) - by Chao Ban

Status of First Author: Student NOT in poster competition, PhD

Authors: Chao Ban, Alan Liu, Tao Li, Yafang Guo

Abstract: The Andes Lidar Observatory (ALO) sodium temperature/wind lidar observed thermosphere sodium layers (TSL) during 6 of the 13 nights of lidar observations between April 15 and 29, 2015. All these TSLs occurred at similar time and altitude (first occurred near 160 km around 0300 UT) and exhibited a downward phase progression which has the same trend as the semidiurnal tides. Especially, between April 17 and 23, TSLs occurred on 5 of the 6 lidar observation nights. Strong equatorial fountain effect was also observed during this period with medium magnetic activity (which may influence the strength of fountain effect). After verifying that the lidar observed winds are similar to the TIEGCM model neutral wind, we used the model neutral wind (zonal/meridional wind) to examine the effect of wind shear on the formation of TSL. The results suggest that the appearance of TSLs cannot be explained by the vertical drift convergence of ions/electrons due to horizontal wind shear. Other mechanisms need to be considered to explain the formation of TSL.

MLTL-13 - Investigation of vertical wavenumber and frequency and spectra of gravity wave motions using vertical wind measurements at Boulder - by Anthony Lima

Status of First Author: Student IN poster competition, Undergraduate

Authors: Anthony Lima, Cao Chen, Xinzhao Chu

Abstract: Vertical wind measurements made with the Sodium Lidar in Boulder, Colorado were used to evaluate the frequency and vertical wavenumber spectra in the mesosphere and lower thermosphere (MLT) region. The spectral characteristics measured in this region can be used to gather insights into the mechanisms for wave damping and dissipation in the upper atmosphere. The observed spectral shape of the vertical wind perturbations can be used to test whether the diffusive filtering plays a crucial role in gravity wave propagation. Measurements can either validate the existing theory or call for a new theory to explain the dissipation of gravity waves.

Mesosphere or Lower Thermosphere General Studies

MLTS-01 - Characteristics of ripple structures revealed from long-term OH airglow images - by Jing Li

Status of First Author: Student IN poster competition, PhD

Authors: Jing Li, Tao Li, Xiankang Dou, Xin Fang, Chao-Yao She, Takuji Nakamura, Alan Manson, Chris Meek, Denise Thorsen

Abstract: Small-scale ripple structures, observed in OH airglow images, are believed to be induced by either dynamic instability due to large wind shear or convective instability due to super-adiabatic lapse rate. Using the dataset observed in the mesopause region by an OH all-sky imager at Yucca Ridge Field Station, Colorado (40.7°N, 104.9°W) from September 2003 to December 2005, we study the characteristics and seasonal variations of ripple structures. Analyzing simultaneous observations of background wind and temperature by a nearby sodium temperature/wind lidar at Fort Collins, Colorado (40.6°N, 105°W) and a Medium Frequency (MF) radar at Platteville, Colorado (40.2°N, 105.8°W), we are able to statistically study the possible relation between ripples and the background atmosphere conditions. Characteristics and seasonal variations of ripples have been presented in detail in this study. Occurrence frequency of ripples exhibits clear seasonal variability, with a peak frequency in autumn. Ripple occurrence shows local time dependence, which is most likely associated with the tides. The lifetime and spatial scales of these ripples are typically 5-20 minutes and 5-10 km respectively, and most of ripples move preferentially toward southward or northward. However, more than half of observed ripples do not advect with background flow. These ripples are possibly not the instability features, but wavebands or wave structures that are hard to be distinguished from the real instability features.

MLTS-02 - Effects of conductivity perturbations in time dependent global electric circuit model - by Jaroslav Jansky

Status of First Author: Non-student, PhD

Authors: Jaroslav Jansky, Victor P. Pasko

Abstract: This study contributes to the understanding of influence of the conductivity perturbations on the ionospheric potential in Earth's global electric circuit (GEC). The conductivity perturbations appearing in middle atmosphere produced by γ -ray bursts from magnetars are studied first. The transient response of the ionospheric potential is modeled in this case and timescales of interest are identified (0.01-10 s). In this case modification of ionospheric potential is small. Additionally, the principal effects of topography and reduction of the conductivity inside the thundercloud are studied. Both of these factors effectively increase the ionospheric potential for a classic source in the GEC represented by a current dipole leading to formation of two main charge centers of the thunderstorm. On the other hand for GEC including topography and conductivity reduction in thunderclouds the contribution of sequence of negative cloud-to-ground lightning discharges to the ionospheric potential is decreased. Simulation results show very good agreement with a simplified approach based on circuit models for conductivity perturbations with horizontal dimensions exceeding 20 km.

MLTS-03 - Analysis of the diurnal variation of the global electric circuit using different numerical models - by Jaroslav Jansky

Status of First Author: Non-student, PhD

Authors: Jaroslav Jansky, Greg M. Lucas, Christina Kalb, Victor Bayona, Michael J. Peterson, Wiebke Deierling, Natasha Flyer, and Victor P. Pasko

Abstract: Diurnal variations of the global electric circuit (GEC) are reflected in diurnal variations of the fair weather electric field measured at the ground. Variations of the fair weather electric field at the ground were first established based on measurements from the Carnegie ship in the first quarter of the 20th century and subsequently linked to diurnal variations of electrified clouds in our atmosphere [e.g., Williams and Mareev, *Atm. Res.*, 135, 208, 2014]. The maximum global coverage of electrified clouds (and thus maximum current source input) to the global electric circuit appears around 19UT when thunderstorms in the Americas are most active.

We aim to create a modelling framework that can represent the GEC. This work has led to several modelling strategies [Jansky and Pasko, *JGR*, 119, 10184, 2014; Bayona et al., *Geosci. Model Dev. Discuss.*, 8, 3512, 2015; Peterson et al., *JAOT*, 32, 1429, 2015; Lucas et al., 120, 12054, 2015; Kalb et al., to be submitted, 2016] that we now compare with the diurnal variation of the GEC [Burns et al., *JAS*, 69, 2062, 2012]. First, we developed GEC models solving continuity equation in 3-D [Jansky and Pasko, 2014; Bayona et al., 2015] and linked them with electric currents obtained from climate models WACCM and INMCM4.0 [Mareev and Volodin, *GRL*, 41, 9009, 2014]. Second, electric fields and currents from electrified weather are retrieved from satellite observations using a methodology developed with direct measurements from high-altitude aircraft [Peterson et al., 2015; Kalb et al., 2016]. The satellite-based approach developed from aircraft overflight data gives a better agreement, in general, with experimental measurements.

MLTS-04 - Earthquake lights: Mechanism of energetic coupling of Earth's crust to the lower atmosphere - by Jaroslav Jansky

Status of First Author: Non-student, PhD

Authors: Jaroslav Jansky, and Victor P. Pasko

Abstract: Co-seismic luminescence, commonly referred to as Earthquake lights (EQLs), is an atmospheric luminous phenomenon occurring during strong earthquakes and lasting from a fraction of a second to a few minutes [e.g., Derr, *Bul. Seismol. Soc. Am.*, 63, 2177, 1973; St-Laurent et al., *Phys. Chem. Earth*, 31

MLTS-05 - Development and Validation of an Airglow Photometer for Upper Atmospheric Chemistry - by Yi Chung Chiu

Status of First Author: Student IN poster competition, Masters

Authors: Yi Chung Chiu, Yi Duann, Loren Chang, J. B. Nee

Abstract: Airglow is a phenomenon caused by chemical reactions in the mesosphere and thermosphere, and can also be used as a proxy to measure important parameters in upper atmosphere. Due to this reason, we have built a simple airglow photometer system and plan to deploy it for long term ground-based observations at Lulin Observatory. We have selected three airglow emission channels (557.7nm, 589nm, 630nm) as our observation target, which have been the subject of several past studies. In order to get reasonable data from our airglow observations, we need to validate all parts of our system, design, calibration, and the data processing procedure.

We have used an integrating sphere to determine the response of our photometer to different levels of irradiance at different channels, and have performed three nights of airglow observations. In the future, we will use our observation results to compare with some atmospheric events and determine chemical changes in the mesosphere and thermosphere. After demonstrating that the data we use is reliable, we will provide long-term observations and monitoring of airglow emission rates and chemical processes over Taiwan.

MLTS-06 - Metal layers in the thermosphere at Arecibo - by Jonathan S. Friedman

Status of First Author: Non-student, PhD

Authors: Jonathan Friedman, Caitlin Kerr, Shikha Raizada, Christiano Brum, Jens Lautenbach, Xinzhao Chu, Frank Djuth, John Mathews

Abstract: We present observations of metal atoms in the thermosphere over Arecibo, with multi-metal lidars and incoherent scatter radar observations.

MLTS-07 - Analysis of Mesospheric Inversion Layers from eCMAM30 (1979 - 2010) - by Christian Tate

Status of First Author: Student IN poster competition, Masters

Authors: Christian Tate and Jian Du-Caines

Abstract: Mesospheric inversion layers (MILs) are a widely studied phenomenon between the stratopause and mesopause that reverse the usual temperature/altitude profile gradient. This investigation uses the extended Canadian Middle Atmosphere Model (eCMAM) data set with thirty years of dynamic and chemical data to explore the amplitude and thickness distributions of long lasting MILs as well as their evolution, duration and scale. Being the first application of eCMAM30 data to study the properties of MILs, this analysis presents an important opportunity to compare results with other General Circulation Models (GCMs). In tentative agreement with WACCM analysis [France et al. 2015] and Lidar observations [Gan et al. 2012, Meriwether and Gerrard 2004], the eCMAM data show similar trends in low and middle latitudes with the seasonal variability most distinct in the tropics during the equinoxes. The statistical properties of amplitude, thickness, duration and scale are also correlated with tides and wave breaking to elucidate the prevailing hypothesis of both middle and high altitude MILs as they manifest in the eCMAM data set.

MLT Other Tidal, PWs, or SSWs

MLTT-01 - A comparison of statistical properties of diurnal tides between eCMAM30 and SABER - by Ashan Vitharana

Status of First Author: Student IN poster competition, Masters

Authors: Ashan Vitharana¹, Jian Du¹, Jens Oberheide²

¹ Department of Physics and Astronomy, University of Louisville, Louisville, KY

² Department of Physics, Clemson University, Clemson, SC

Abstract: In this research we investigate and compare statistical characteristics of the diurnal tides and illustrate how these statistical characteristics change with season, latitude and altitude from the troposphere to the thermosphere/ionosphere, using data from the extended Canadian Middle Atmosphere Model (eCMAM30) run (1979-2010) and the Sounding of the Atmosphere using Broadband Emission Radiometry

(SABER) instrument on NASA's TIMED (Thermosphere Ionosphere Mesosphere Energetics Dynamics) satellite. In this comparison statistical mean, standard deviation, cross correlation, frequency probability density functions (PDFs) and other statistical methods were developed as a function of altitude, latitude and time to examine the underlying statistics governing the short-term and long-term tidal variability and to what extent these properties changes temporally and spatially between eCMAM30 and SABER.

MLTT-02 - Physical Mechanisms of Seasonal Variation of DW1 from the Stratosphere to Thermosphere in eCMAM30 - by Hongping Gu

Status of First Author: Non-student, PhD

Authors: Hongping Gu, Jian Du

Abstract: The migrating diurnal tide (DW1) is one of the strongest-amplitude global scale perturbations at low latitudes of the middle and upper atmosphere. The physical mechanisms that determining the seasonal variations of DW1 are examined at three atmospheric altitudes – 45, 95 and 165 km, which represent stratosphere, mesosphere and thermosphere respectively, using a 30-year (1979-2010) output from the extended Canadian Middle Atmosphere Model (eCMAM). The results show that in the stratosphere, the pressure gradient force and Coriolis force are the dominant terms in the zonal momentum budget and exhibit similar seasonal variations as the tide whereas advection and model physics play insignificant role. The seasonal variation of DW1 in the thermodynamic budget is mainly controlled by the short-wave heating and adiabatic heating terms. In the mesosphere, besides of the classic terms (PGF and Coriolis force), advection and curvature terms are also important for the seasonal variation of DW1. In the thermodynamic budget, both adiabatic and advection are important. All of the model physics and diabatic terms do not exhibit similar seasonal variations as the tide. For the thermosphere, model physics (mainly ion drag) becomes the second largest term to the classic terms although advection is also important. The short-wave heating is the most important term in the thermodynamic budget besides adiabatic and advection terms. This study shows the complexity of the main physical mechanisms modulating seasonal variation of tides at different regions of the atmosphere.

MLTT-03 - Parameterized Gravity Wave Effects on Major Tidal Modes in eCMAM and WACCM - by Ryan Agner

Status of First Author: Student IN poster competition, PhD

Authors: Ryan Agner

Abstract: Thermal tides are a major feature of the earth's atmosphere and their interactions with smaller scale dynamics such as gravity waves are not well understood. In most Global Circulation Models gravity waves are parameterized, which further adds to the uncertainty of describing such interactions. In this study, the extended Canadian Atmospheric Model (eCMAM) and the Whole Atmosphere Community Climate Model (WACCM) are used to study the differences in major tidal modes between the models, with the focus on the impact of gravity waves on these differences, and their relationship to the differences in gravity wave parameterization schemes. For each tidal mode, all terms in its corresponding momentum equation are analyzed and compared. Several properties of the parameterization schemes such as propagation direction relative to the wind and dissipation altitudes are studied for their contributions.

MLTT-04 - Vertical structures of temperature change in the mesosphere and lower thermosphere regions during stratospheric sudden warnings - by Jeong Han Kim

Status of First Author: Non-student, PhD

Authors: Jeong-Han Kim, Geonhwa Jee, Young-In Won, Back-Min Kim, Have-Sun Choi, and Seong-Joong Kim

Abstract: We analyze the temperatures obtained from Fourier Transform Spectrometer (FTS) and Micro Limb Sounder (MLS) onboard Aura satellite, and the polar cap index (PCI) of MERRA re-analysis for two major Stratospheric Sudden Warmings (SSW) on Jan. 2006 and Jan. 2009, in order to investigate the vertical structure changes of the stratospheric and mesospheric temperatures with time. For our purpose, we compute the height profiles of the correlation coefficients between daily MLS temperature anomalies of 55 height levels, which are averaged over 65°N latitude, and MERRA 10 hPa PCI anomalies for three periods divided into pre-, main- and post- phases of two major SSWs. In this study, we present our results and discuss about the difference between the observation and model simulation by comparing our results with those from the temperatures of WACCM simulation.

MLTT-05 - Nonmigrating tidal impact on the CO₂ 15 μm infrared cooling of the lower thermosphere over one solar cycle - by Nirmal Nischal

Status of First Author: Student IN poster competition, Masters

Authors: Jens Oberheide, Martin G. Mlynczak, Linda A. Hunt, Astrid Maute

Abstract: We explore the impact of nonmigrating tides originating from tropospheric weather system on the 15 μm CO₂ infrared cooling of the lower thermosphere over a full solar cycle. Tidal diagnostics of SABER CO₂ 15 μm volume emission rate (VER) data shows that the CO₂ cooling rate amplitudes for the DE2 and DE3 components are on the order of 15-60% relative to the monthly means, depending on season. Consequently, upward propagating nonmigrating tides result in a substantial modulation of the energy budget of the lower thermosphere. Supporting photochemical tidal modeling reproduces the general amplitude structures and phases. The main tidal coupling mechanism in the MLT region during solar minimum is the temperature dependence of the collisional excitation of the CO₂ (01101) fundamental band transition (v₂). However, the response to neutral density variations becomes as important as temperature above 115 km and as such explains an unexpected tidal phase behavior in the observation. The contribution of vertical advection is comparatively small. A sensitivity analysis of the modeled DE2 and DE3 CO₂ VER tides and tidal driving mechanisms to the specific choice of mean temperature, atomic oxygen, and CO₂ density suggests that the current uncertainties in background temperature and atomic oxygen used for the photochemical modeling do not impact our conclusion about the relative importance of the tidal coupling. The paper also discusses how the relative importance of the tidal coupling mechanisms changes as a function of latitude and solar cycle, in order to fully quantify the response of the CO₂ 15 μm infrared cooling of the lower thermosphere to tropospheric tides.

Sprites

SPRT-01 - Numerical and analytical studies of critical radius in spherical and cylindrical geometries for corona discharge - by Jacob Allen Engle

Status of First Author: Student IN poster competition, Undergraduate

Authors: J. A. Engle; J. A. Riousett

Abstract: The ability to protect modern infrastructure as effectively as possible from lightning strikes has become essential with the development of complex electronic, communication, and power systems (Riousett, 2010). In order to determine the most effective geometry of a lightning rod, one must first understand the physical difference between their current designs. Benjamin Franklin's original theory of sharp tipped rods suggests an increase of local electric field, while Moore et al.'s (2000) studies of rounded tips evince an increased probability of strike (Moore et al., 2000; Gibson et al., 2009). At the beginning of the connection process between the descending lightning channel and the upward connecting leader, there is the formation of a "precursor" plasma discharge around the rod in the form of an ionization front (Golde,

1977). In this analysis, the plasma discharge is produced between two electrodes with a high potential difference, resulting in ionization of the neutral gas particle and creating a current in the gas medium. This process, when done at low current and low temperature, creates a corona, or “glow” discharge, which can be observed as a luminescent emission. The Cartesian geometry known as Paschen, or Townsend, theory is particularly well suited to model experimental laboratory scenario, however, it is limited in its applicability to lightning rods. Franklin’s sharp tip and Moore et al.’s (2000) rounded tip fundamentally differ in the radius of curvature of the upper end of the rod. As a first approximation, the rod can be modelled as an equipotential conducting sphere above the ground. Hence, we expand the classic Cartesian geometry into a spherical geometry, where a small radius effectively represents a sharp tip rod, while larger, centimeter-scale radius represents a rounded, or blunt tip. Empirical investigations of lightning-like discharge are of a limited in size. They are typically either a few meters in height, or span along the ground to allow the discharge to occur over a large distance. Yet, neither scenarios account for the change in neutral charge density, which conditions the reduced electric field, and therefore hardly reproduce the condition of discharge as it would occur under normal atmospheric conditions (Raïser, 1991). In this work we explore the effects of shifting from the classical parallel plate analysis to spherical and cylindrical geometries more adapted for studies of lightning rods. Utilizing Townsend’s equation for corona discharge, we estimate a critical radius and minimum breakdown voltage that allows ionization of the air around a lightning rod. We solve the problem both numerically and analytically to present simplified formulas for each geometry, and discern a definitive effective design. The development of a numerical framework will ultimately let us test the influence of parameters such as background ionization, initiation criterion, and charge conservation on the values of the critical radius and minimum breakdown voltage.

References [1] C. B. Moore, W. Rison, J. Mathis and G. Aulich (2000), “Lightning rod improvement studies,” *J. Appl. Meteor.* 39 (5) 593–609. [2] A. S. Gibson, J. A. Riouset, and V. P. Pasko (2009), Minimum breakdown voltages for corona discharge in cylindrical and spherical geometries, *NSF EE REU Penn State Annual Research Journal*, 7, 1–17. [3] R. H. Golde, ed., *Lightning*, vol. 1: *Physics of Lightning*, Academic Press, London, UK; New York, NY, 1977. [4] Y. P. Raïser, *Gas Discharge Physics*. Berlin: Springer-Verlag, 1991.

SPRT-02 - The Electrical Impact of Sprite Halos on the Nighttime Lower Ionosphere - by Mohammad Ahmad Salem

Status of First Author: Student IN poster competition, PhD

Authors: Mohammad A. Salem , Ningyu Liu , Hamid K. Rassoul

Abstract: Significant electrostatic (ES) fields although not strong enough to produce transient luminous events (TLEs) such as elves, halos, and sprites, could be established in the lower ionosphere by underlying thunderstorms [Salem et al., *GRL.*, 42(6), 2015]. We recently found that the nighttime lower ionospheric height measured by using the VLF wave reflection technique can be increased due to the effects of the thunderstorm ES field [Salem et al., *GRL.*, 43(1), 2016].

In this study, we continue further to investigate the ionospheric effects of the quasi-electrostatic (QE) fields of cloud-to-ground (CG) lightning flashes, which can be much stronger than the thunderstorm ES field and sometimes trigger halos. Halos are relatively homogeneous glows centered on 75-85 km altitude with a horizontal extent of tens of kilometers and a vertical thickness of several kilometers. They typically appear within a few milliseconds of intense CGs.

Our study is conducted by combining a one dimensional plasma discharge fluid model with a simplified ionospheric ion chemistry model described by Liu [JGR., 117, A03308, 2012]. The modeling results of the lower ionospheric response to the lightning-induced QE fields are analyzed to investigate the role of halos in early VLF perturbations (early VLF events). Early VLF events have been observed coincidentally in time with a variety of TLEs [e.g., Moore et al., JGR, 108, 1363, 2003; Marshall et al., JGR, 111, D19108, 2006; Cotts and Inan, GRL, 34, L14809, 2007; Haldoupis et al., JGR, 14, A00E04, 2009; Haldoupis et al., GRL, 39, L16801, 2012]. However, the physical processes responsible for their production have not yet

been conclusively identified. Finally, we compare the modeling results with recent studies on the recovery timescales of early VLF events [e.g., Kotovsky and Moore, GRL 43(3), 2016].

Stratosphere Studies and Below

STRA-01 - The northern stratospheric temperature response to MJO in cases SSW occurs or not - by Chengyun Yang

Status of First Author: Non-student, PhD

Authors: Chengyun Yang, Tao Li and Xiankang Dou

Abstract: Using ERA-Interim, we investigated the effects of the Madden-Julian oscillation (MJO) on the mid-winter stratosphere in the northern hemisphere, particularly in case when SSW happen or not. In the years in which SSW occurs (SSW years hereafter), the polar cap temperature response to MJO is stronger than that in the years in which SSW do not occur (non-SSW years). In SSW years, the northern polar temperature becomes warmer than normal in upper stratosphere in 15-20 days after the phase 3 (P3) of MJO. The anomalous warm then propagate downward to 10-100hPa in 30-40 days after the phase 3. On the other hand, in non-SSW years, the northern polar temperature is cooler in 15-20 days after MJO P3 and becomes warmer later. The response of northern polar temperature to phase 7 of MJO is opposite to that response to MJO P3. The anomalous Eliassen-Palm flux and its divergence indicate the planetary waves (PWs) enhance in 0-10 days and in around 30 days after MJO P3 in either SSW or non-SSW years. During SSW years, the wavenumber 1 (WN1) PWs significantly enhanced in 0-10 days after MJO P3 and become weaker and insignificant soon, while WN2 PWs enhanced in 30 days after MJO P3. The PWs response to MJO is different in non-SSW years: the WN2 PWs significantly enhanced first (in 0-10 days after MJO P3) and become weaker and insignificant soon, while WN1 PWs enhanced in 30 days after MJO P3.

STRA-02 - Thunderstorm Charge Structures Producing Negative Gigantic Jets - by Levi Boggs

Status of First Author: Student IN poster competition, PhD

Authors: Levi Boggs, Ningyu Liu, Hamid Rassoul

Abstract: Lightning discharges that escape the upper region of the thundercloud and travel upward to the lower ionosphere (80 km) are known as gigantic jets [Pasko et al., Nature, 416, 152-154, 2002; Su et al., Nature, 423, 974-976, 2003]. They often are produced by oceanic storms [Chen et al., JGR, 1113, A08306, 2008] and are usually of negative polarity, transferring negative charge upward. These discharges electrically couple the upper troposphere and the lower ionosphere. Gigantic jets are often very powerful and have been found to transfer very large amounts of charge to the ionosphere on a timescale of hundreds of milliseconds to seconds [Liu et al., Nat. Comm., 6, 5995, 2015].

The typical thunderstorm has a tripolar charge structure, with large upper positive charge, large middle negative charge, and small lower positive charge. An upper negative screening layer can also be found at the upper thundercloud boundary [Krehbiel et al., Nat. Geosci., 1, 233-237, 2008; Rioussset et al., JGR, 115, A00E10, 2010]. Most lightning discharges are intracloud (IC) flashes between the upper and middle charge regions. However, if the upper positive charge region is weakened, then an IC flash can escape the upper positive charge and become a gigantic jet [Krehbiel et al., 2008; Rioussset et al., 2010]. This takes place when the upper negative screening layer mixes with the upper positive charge, resulting in a charge imbalance between the middle negative and upper positive charge regions. Gigantic jets have been found in environments that exhibit strong external wind shear near the upper thundercloud boundary [Lazarus et al., JGR Atmos., 120, 8469- 8490, 2015]. This strong wind shear likely aids in mixing the upper negative screening layer with the upper positive charge, facilitating the formation of gigantic jets.

The work we present here includes a detailed charge structure analysis of four gigantic jet producing thunderstorms. The analysis involves combining dual- polarization radar, very high frequency and low frequency lightning, and balloon radiosonde data. Our results show that the charge structure of the gigantic jet producing thunderstorms is very different from the typical tripolar thunderstorm charge structure. We will discuss what meteorological processes form these charge structures and what makes them unique.

Agner, Ryan, 25
Aguilar, Jaime, 14
Amaro-Rivera, Yolian, 17
Azeem, Irfan, 7

Ban, Chao, 21
Boggs, Levi, 28
Bruntz, Robert, 15

Cao, Bing, 10
Chang, Loren, 1
Chen, Cao, 15
Chiu, Yi Chung, 23

Elliott, Shayli, 18
Engle, Jacob, 26

Friedman, Jonathan, 24

Galindo, Freddy, 12
Gasperini, Federico, 5, 6
Grawe, Matthew, 4
Gu, Hongping, 25
Guo, Yafang, 21

Haaser, Robert, 2
Hawkins, Jessica, 6
Hooser, Preston, 9

Inonan, Marcos, 7

Jansky, Jaroslav, 22, 23
Jones Jr., McArthur, 4
Juarez Madera, Diana, 12

Kavanagh, Andrew, 16
Kim, Gawon, 10
Kim, Jeong Han, 25
Krier, Christopher, 2

Lai, Jih-Chin, 8
Lautenbach, Jens, 10

Li, Jing, 22
Li, Jintai, 9
Lima, Anthony, 21
Limonta, Lorenzo, 13
Lin, Cissi, 5
Lobay, Thomas, 14
Lu, Xian, 20
Lucas, Greg, 6

McCormick, Jackson, 8
McInerney, Joe, 3
McLaughlin, Pattilyn, 13
Mehta, Dhvanit, 15
Mesquita, Rafael, 3
Mixa, Tyler, 16
Moser, David, 19

Navarro, Luis, 19
Nguyen, Vu, 3
Nischal, Nirmal, 26
Nuttall, Andrew, 11

Price, Jonathan, 17

Qiao, Shuai, 20

Salem, Mohammad, 27
Salinas, Cornelius Csar Jude, 1
Sox, Leda, 17
Sugar, Glenn, 12

Talaei, Ahmad, 13
Tarnecki, Liane, 11
Tate, Christian, 24

Vitharana, Ashan, 24

Wickwar, Vincent, 18

Yang, Chengyun, 28

Zhao, Jian, 19